GEOLOGICA CARPATHICA, AUGUST 2006, 57, 4, 227–242

Electron microprobe dating of monazite from the Nízke Tatry Mountains orthogneisses (Western Carpathians, Slovakia)

IGOR PETRÍK[1], PATRIK KONEČNÝ[2], MARTIN KOVÁČIK[2] and IVAN HOLICKÝ[2]

[1]Geological Institute, Slovak Academy of Sciences, Dúbravská cesta 9, P.O. Box 106, 840 05 Bratislava, Slovak Republic; geolpetr@savba.sk
[2]Geological Survey of Slovak Republic, Mlynská dolina 1, 817 04 Bratislava, Slovak Republic

(Manuscript received September 12, 2005; accepted in revised form March 16, 2006)

Abstract: The age and composition of monazite from ortho- and paragneisses of the Nízke Tatry Mts (Low Tatra Mts) was studied by microprobe chemical method. The monazite shows relatively uniform composition characterized by substitutions to xenotime (7–10 mol. %) and brabantite (6–11 mol. %), much less to huttonite (0–2 mol. %). Biotite-hosted monazite is commonly overgrown by thin REE-epidote rims, in a less foliated sample it is apparently unstable and breaks down to apatite, REE-epidote and a Th-silicate (huttonite?). Empirical thermometers based on Y in monazite give 600–650 °C for xenotime-bearing samples. Extensive dating by Cameca SX-100 microprobe yielded a range of ages: the majority of data cluster around 340–360 Ma indicating either a Variscan origin of orthogneisses or strong reworking of an older granitic protolith. Because monazite recrystallized at subsolidus temperatures it seems to have failed to record a magmatic age. However, an Ordovician core (ca. 475 Ma) was found in one monazite grain from mylonitic Bystrá augengneiss. This partially melted orthogneiss also contains younger monazites (320–330 Ma) which probably recrystallized during this Variscan event. Decompression-related muscovite melting was probably the reason for the partial melt formation. Metamorphic monazites from medium-grade biotite gneisses also record several ages: old inherited cores (450 Ma) and metamorphic events occurring probably at ca. 390, 350 and 330 Ma.

Key words: Western Carpathians, Nízke Tatry, age, microprobe dating, gneiss, orthogneiss, monazite.

Introduction

Orthogneiss, an important rock type occurring in the Western Carpathian basement, can be found in all main tectonic units but the most extensive occurrence is in the Nízke Tatry Mts (Low Tatra Mts). Both banded (stromatite) and augengneiss (ophthalmite) varieties occur together with paragneisses and amphibolites. While earlier authors treated orthogneisses as migmatites (e.g. Miko & Lukáčik 1983), the interpretations published in recent years prefer their granitic protolith and most authors consider them ductilely deformed syn-tectonic granitoids (Adamija et al. 1992; Janák 1994; Petrík et al. 1998; Poller et al. 2000, 2001; Putiš et al. 2003). The first trace element data on orthogneisses were brought by (Méres & Hovorka 1992), who compared them with post-tectonic Variscan granitoids. Petrík et al. (1998) studied their mineral composition, especially K-feldspars. The summary of the existing data was recently presented by Kohút (2004). Paragneisses were studied as part of the Nízke Tatry metamorphic complex by Spišiak & Pitoňák (1990), who interpreted them as a product of metamorphism of a mixed protolith with variable extent of terrigeneous and volcanogeneous material.

The presence of monazite, a main light rare earth element (REE) mineral of orthogneisses enables their dating by a chemical method (Montel et al. 1996). Monazite contains enough Th and U to produce radiogenic Pb in amounts measurable by microprobe, while containing no common Pb (Parrish 1990). The electron microprobe dating method has been successfully applied to various granitoids (Finger & Broska 1999; Finger & Faryad 1999; Finger et al. 2003) or metapelites (Konečný et al. 2004) in the Western Carpathians.

In this paper we present results of monazite geochronological study showing the main features of compositional variations and geochronological history as recorded by various monazite domains and yielding several Variscan and pre-Variscan ages.

Monazite stability

Monazite is able to record a complex polymetamorphic history and is commonly used for isotopic dating of metamorphic and magmatic events. Diffusion of radiogenic lead is negligible even at high temperatures above 900 °C (Braun et al. 1998; Cherniak et al. 2004), so individual metamorphic growth zones can be dated (Crowley & Ghent 1999). Monazites moreover commonly contain identifiable old inherited cores. New monazite may grow due to the change of fluid regime mainly from apatite and allanite, a source of LREE (Simpson et al. 2000; Foster et al. 2002). This process is opposite to the breakdown of monazite observed in various metagranites (Finger et al. 1998; Broska & Siman 1998). Monazite can form new domains overgrowing older cores or it may recrystallize after previous partial dissolution (Crowley & Ghent 1999). Dissolution and reprecipitation is an important growth mechanism because (1) it does not require a net monazite growth, and (2) new monazite may date the process without complete resetting by volume diffusion of old lead, which is according to most authors negligible. Harlov et al. (2005) studied this process in experimentally metasomatized apatite. They found that replacement occurs after a moving reaction front along which new monazite grows. Micro- and nanoporosity allows fluids to permeate through metasomatized areas as fluid-aided diffusion. Monazites commonly show internal zonation or inhomogeneities visible in BSE images. These are usually caused by increased Th (bright domains) or Y (dark domains). The increase of Y, heavy REE and U results mainly from the escape of light REE and resulting decrease of crystallographical sites (Poitrasson et al. 1996). At 350 °C in acid and oxidation environment monazite may break down to apatite and allanite (Poitrasson et al. 2000). This alteration was observed in the Carpathians and Alps at higher P-T conditions (Finger et al. 1998; Broska & Siman 1998).

Vavra & Schaltegger (1999) demonstrated Permian and Triassic rejuvenation of monazite by lead loss, which however was not caused by diffusion but by the activity of fluids. The resetting of monazite by recrystallization may occur below its closing temperature, even at 350–400 °C (Townsend et al. 2000).

Geological setting

Straddling the main Alpine superunits of the Western Carpathians — the Tatric and Veporic Units, the mega-horst of the Nízke Tatry Mountains is one of the largest mountain ranges of the Western Carpathians (Fig. 1). The studied rocks come from the pre-Mesozoic basement of its Tatric part. The basement core consists of granitoids, high-grade orthogneisses, paragneisses, amphibolites and ultramafic rocks. The post-tectonic tonalites and granodiorites (Ďumbier and Prašivá type) forming the northern belt of the mountains are separated from the gneisses and amphibolites of the southern belt by a nebulite zone (Bezák & Klinec

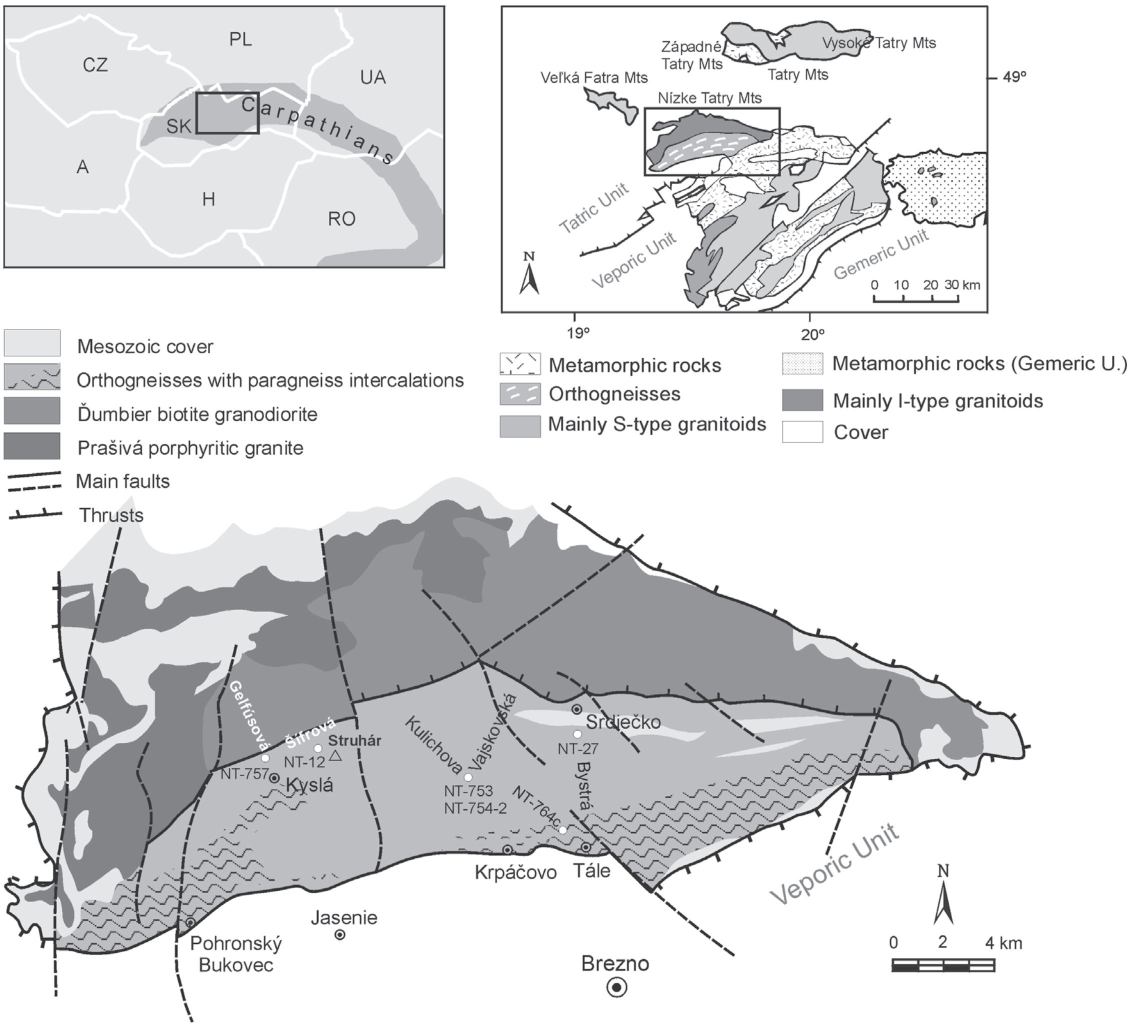

Fig. 1. Sketch geological map of the Nízke Tatry Mts (adapted according to Bezák & Biely 1998). Sample localities and positions of some valleys (e.g. Gelfúsová) are also shown.

1983). The whole complex forms the upper Variscan tectonic unit with amphibolites occurring at its sole. Madarás et al. (1999) recognized in orthogneisses two deformation events. The first event produced the foliation S_0 (magmatic) and S_1 (metamorphic) related to syn-metamorphic intrusion into a shear zone. Kinematic indicators show prevailing top-to-SE thrusting, the same as was found in the Západné Tatry Mts (Western Tatra Mts) (Fritz et al. 1992). S_2 foliations are mylonitic and deformations indicate a temperature of more than 450 °C. They are attributed to the second deformation phase related to the collapse of thickened Variscan crust (Madarás et al. 1999; Putiš et al. 2003), which was accompanied by partial anatexis and retrogression.

The P-T conditions of metamorphism in the Nízke Tatry are not yet precisely established. They were estimated for massive garnet-clinopyroxene metabasites at 790–830 °C and 1300–1500 MPa (Janák et al. 2000b). The boudins of these rocks occurring in banded amphibolites were identified as retrograde eclogites in the adjacent Western Tatra Mts (Janák et al. 1996). Few existing data from metapelites yield conditions of 620–660 °C and 320–360 MPa (Janák et al. 2000a). However, high-grade metamorphism and melting can be inferred from the presence of sillimanite and sporadic kyanite in paragneisses.

Orthogneisses were dated by conventional zircon dating, which gave 381±6 Ma (LI, UI 1232±31 Ma, Putiš et al. 2003). $^{40}Ar/^{39}Ar$ dating of orthogneiss muscovites yielded 331±2 Ma (Dallmayer et al. 1993).

Methods

The new data presented in this work were obtained using the microprobe Cameca SX-100 in the laboratory of Geological Survey of the Slovak Republic in Bratislava. To achieve a sufficient number of counts with the lowest rate of surface destruction we used the following conditions (Konečný et al. 2004): 15 kV accelerating voltage, 80–150 nA sample current, 75–130 s counting time and beam diameter about 5 μm. The PAP correction procedure was used for the conversion of counts to wt. %. Most elements were measured using the large crystals (LPET, LTAP) which are about 8 times more sensitive than conventional ones (Table 1). To avoid or minimize the effect of interferences the lines of higher order were chosen.

Interferences $PbM\alpha_1$ with $Y\xi_1$ and $UM\alpha_1$ with $ThM\beta 1$ were corrected by K_{ovl} factor obtained as the average from repeatedly measured YPO_4 and ThO_2 standards (at least 5–10 times). The readiness of the microprobe for dating was proved by dating of five monazite standards of various ages from 1840 to 77 Ma. The acceptable deviation from a true age is ±5 Myr for monazite standards younger than 500 Ma, and ±20 Myr for the oldest monazite standard (1840 Ma).

The histogram base of monogenetic age monazite standards as revealed by multiple measurements is about 60 Ma for an average standard deviation ±15 Myr (1σ). Therefore, the only events recorded by a polygenetic monazite population differing by >30 Myr may be successfully distinguished (Konečný et al. 2004). Weighed averages were calculated using Isoplot/Ex v. 2.49 (Ludwig 2001).

Table 1: List of standards, element lines and crystals used for monazite measurement. All lines are of the first order (according to Konečný et al. 2004).

Element	Line	Crystal	Standard
Pb	Mα	LPET	PbS
U	Mβ	LPET	UO_2
Th	Mα	LPET	ThO_2
Y	Lα	LPET	YPO_4
Ce	Lα	LIF	$CePO_4$
La	Lα	LLIF	$LaPO_4$
Gd	Lα	LLIF	$GdPO_4$
Yb	Lα	LLIF	$YbPO_4$
Sm	Lβ	LLIF	$SmPO_4$
Pr	Lβ	LLIF	$PrPO_4$
Er	Lβ	LLIF	$ErPO_4$
Nd	Lβ	LLIF	$NdPO_4$
Lu	Lβ	LLIF	$LuPO_4$
Ho	Lβ	LLIF	$HoPO_4$
Dy	Lβ	LLIF	$DyPO_4$
Tb	Lα	LLIF	$TbPO_4$
Al	Kα	TAP	Al_2O_3
Si	Kα	TAP	wollastonite
P	Kα	LPET	apatite
Ca	Kα	LPET	wollastonite

Rock characterization

Orthogneisses are medium- to coarse-grained rocks with stromatitic or ophthalmitic character depending on the presence of K-feldspar "augen". In contrast to post-kinematic Variscan granitoids occuring to the north (Ďumbier type) they have banded appearance due to 1–2 mm thick biotite bands alternating with quartz–feldspar bands. The K-feldspar occurs as porphyroblasts (originally phenocrysts) ranging in size from several millimeters to 6 cm. Due to shearing they commonly form more or less overgrown augen. In some coarse-grained varieties the banding is discontinuous, and the rock acquires a more granitic appearance. The orthogneiss complex contains abundant migmatitic varieties and paragneiss xenoliths forming various inhomogeneities and schlieren. The xenoliths are represented by a massive, fine-grained biotite-garnet gneiss (e.g. in Kyslá area). Locally, medium-grained metapelites were found containing garnet and sillimanite (to the E of Krpáčovo), Fig. 1.

The chemical composition of orthogneisses is monotonous which is true also for orthogneisses from other mountain ranges (Kohút 2004). Relatively acid and peraluminous composition, the presence of two micas and a moderate to low content of accessories suggest a metasedimentary source rock of granitoid protolith. The only special feature of Nízke Tatry orthogneisses are increased concentrations of W, which are 3–5 times higher than in Ďumbier granitoids. Iron-rich biotite, the lack of magnetite and presence of pyrite indicate a reduced character of magma. The rare earth elements (REE) are controlled by monazite, apatite and xenotime. Whole rocks have dis-

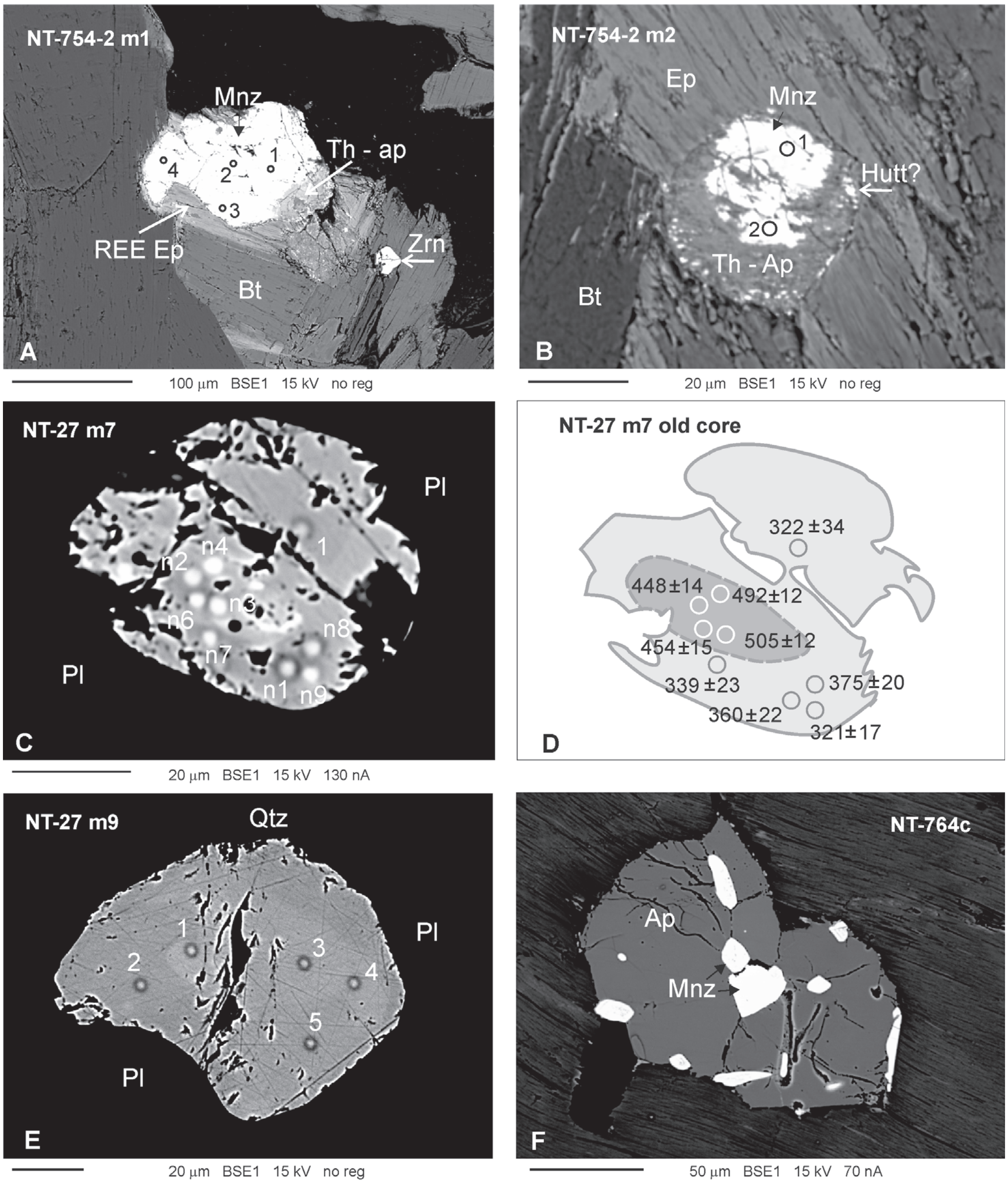

Fig. 2. BSE images of monazite from orthogneisses NT-754-2, 27 and muscovite gneiss NT-764c. Points refer to Table 2. Sketch of the old core in monazite m7 is shown in (D) with point ages. (A–B) show the breakdown of monazite to Th-apatite, rimmed by a Th mineral (huttonite?) and REE-epidote.

tinctly elevated contents of heavy REE (Gd-Lu), showing flat patterns $(La/Yb)_N = 5–10$. The trace element composition of paragneisses is not known.

Petrography and localization of samples

Orthogneisses are represented by samples NT-12, NT-27, NT-754-2, NT-753, paragneisses by samples NT-757, NT-764c.

Sample NT-12: Foliated biotite orthogneiss. SE slope of Struhár Mts elevation 1220 m a.s.l. Fine discontinuous bands (< 1 mm) are defined by biotite. The rock has the composition of tonalite with sub- to anhedral texture and indistinctly foliated fabric. The biotite is fresh, fine, subhedral, dark-red to pale-yellow. The plagioclase is anhedral, zoned with basicity An_{30-34} in cores and An_{20} at rims. The quartz is anhedral, shows undulous extinction, intergrown with plagioclase. Only rare interstitial K-feldspar is present, while muscovite is absent in the rock. Abundant accessories are represented by apatite, monazite and zircon, mostly enclosed in biotite, where they form distinct pleochroic halos. Biotite-hosted monazite is commonly surrounded by REE-epidote coronas (Fig. 3D). The rock is only weakly mylonitic.

Sample NT-27: Coarsely banded mylonitic orthogneiss with sporadic K-feldspar augen 1–3 cm in size. Bystrá dolina Valley, large outcrop on the W side of the road Tále–Srdiečko, elevation 960 m a.s.l. The rock has the composition

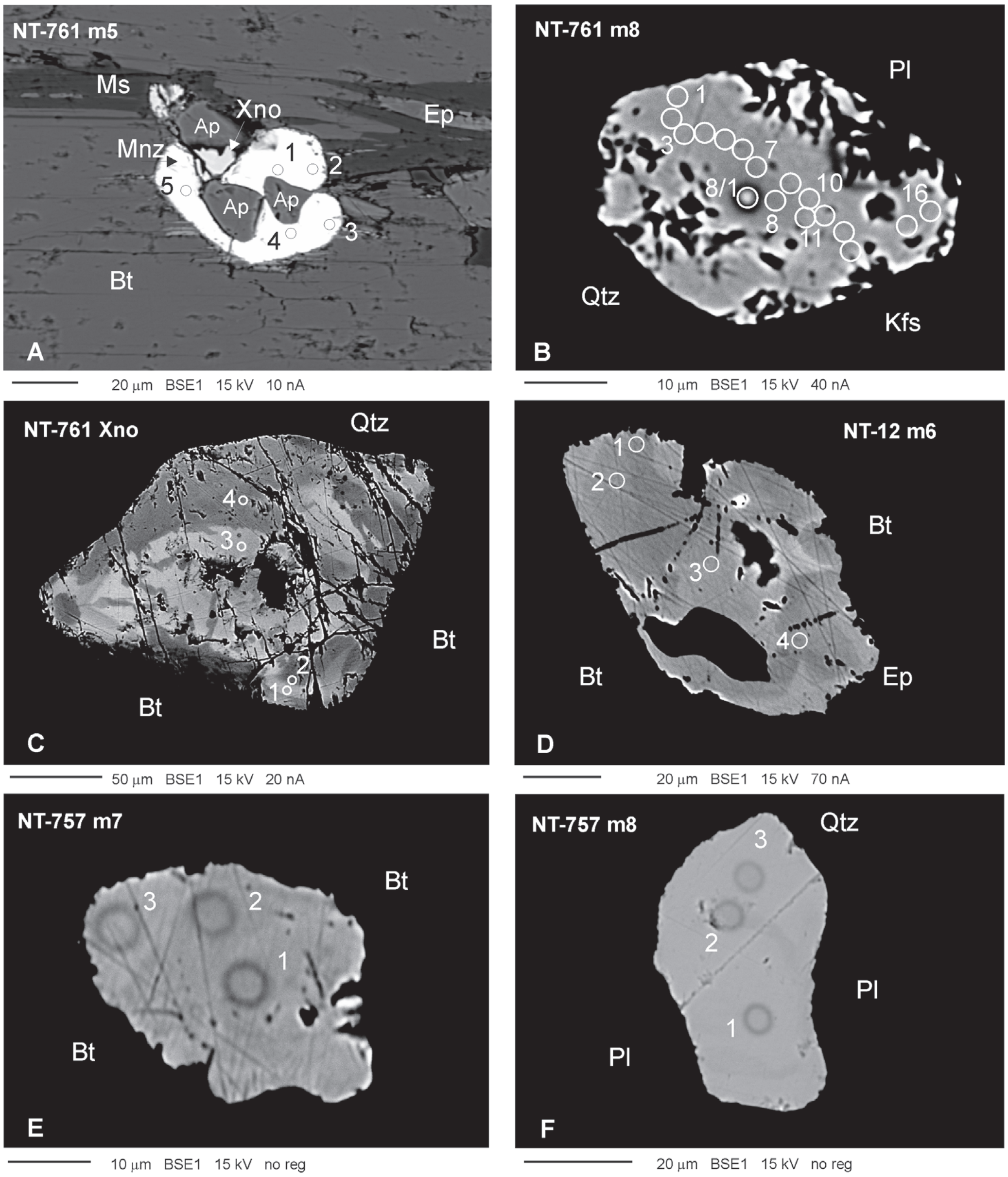

Fig. 3. BSE images of selected studied monazites (A,B,D–F) and xenotime (C) from orthogneisses NT-761, 12 and paragneiss NT-757. The numbers of analysed points correspond to Table 2.

of muscovite-biotite granodiorite. It is distinctly foliated and mylonitic. Two varieties of K-feldspar (30 %) can be recognized: 1 — Large perthitic phenocrysts, which enclose small euhedral plagioclases. The big augen consist of several individuals separated by quartz septa. 2 — Interstitial, non-perthitic K-feldspar associated with quartz drops in anhedral pools probably resulting from partial melting. The plagioclase is sub- to anhedral, unzoned intergrown with quartz. Basicity is An_{30-26}. Quartz shows undulouse extinction, in places dynamically recrystallized. The biotite (10–15 %) is subhedral, dark red-brown to straw-yellow, relatively fresh. The muscovite (3–4 %) is usually intergrown with biotite showing exsoluted rutile, occasionally is cross-oriented. The accessories are represented by apatite, zircon and monazite. The monazite is hosted in biotite, quartz, plagioclase and muscovite (Fig. 2C–E). The biotite-hosted monazite has thin REE-epidote rims. A small amount of an ore mineral (pyrite?) is also present.

Sample NT-753: Biotite schlier from orthogneiss. A cliff 5 m above road at the beginning of Kulichova dolina Valley to Vajskovská dolina Valley, 758 m a.s.l. The rock is composed mainly of biotite (90 vol. %), quartz (5–10 %) and plagioclase (2–3 %). The biotite is dark red-brown to pale yellow, fresh but strongly deformed. Along cleavage it contains small exsolved titanites. The quartz shows undulous extinction, and the plagioclase is strongly sericitized. The accessories especially big columnar apatite and zircon are abundant in biotite. Monazite is, however, not common.

Table 2: Representative analyses of studied monazites and xenotime. The crystalochemical formulae are based on 16 oxygens. Temperatures (°C) calculated according to Pyle et al. (2001) are given for samples NT-27 and 761. **n.d.** — element below detection limit, **n.a.** — element not analysed. *Continued on the next page.*

Sample	NT-757	NT-757	NT-757	NT-757	NT-757	NT-12	NT-12	NT-12	NT-754-2	NT-754-2	NT-754-2	NT-754-2	NT-754-2
Grain	m7-1	m7-3	m8-1	m8-2	m8-3	m6-1	m6-3	m6-4	m1-1	m1-2	m1-3	m2-1	m2-2
Age	455.6	394.7	381.6	442.5	383.4	385.3	320.2	310.3	379.7	347.8	368.0	405.0	341.7
P_2O_5	28.05	28.01	27.85	27.94	27.61	27.55	27.22	27.78	27.07	27.23	26.57	26.60	26.63
SiO_2	0.20	0.18	0.20	0.15	0.15	0.31	0.47	0.32	0.41	0.29	0.85	0.70	0.73
CaO	0.77	1.15	1.04	0.76	0.99	0.67	0.96	0.71	0.90	1.16	1.04	1.07	1.31
ThO_2	3.11	3.92	4.19	2.39	3.69	2.74	4.63	2.99	4.76	5.17	7.22	6.12	6.56
UO_2	0.61	0.92	0.91	1.05	0.88	0.66	1.14	0.74	0.49	0.80	0.32	0.28	0.37
PbO	0.10	0.12	0.12	0.11	0.11	0.08	0.11	0.07	0.11	0.12	0.13	0.12	0.11
La_2O_3	12.90	13.11	12.96	13.12	13.14	13.16	12.25	12.90	12.85	12.52	12.19	12.23	11.84
Ce_2O_3	27.66	27.95	27.60	28.12	28.03	28.09	25.84	27.59	27.54	26.79	26.64	26.85	25.63
Pr_2O_3	3.13	3.08	3.32	3.10	3.25	3.25	3.00	3.11	3.03	3.20	3.12	3.21	3.04
Nd_2O_3	12.99	12.78	13.06	12.57	12.82	11.74	11.14	11.95	11.60	11.67	11.03	11.72	11.77
Sm_2O_3	2.44	2.25	2.32	2.14	2.24	2.12	2.06	2.13	2.19	2.26	1.99	1.99	2.04
Gd_2O_3	2.39	2.25	1.94	2.24	2.13	2.11	2.14	2.13	2.03	2.13	1.98	1.89	2.07
Er_2O_3	n.d.	n.d.	0.32	n.d.	0.18	0.10	0.32	0.14	0.02	0.06	0.12	0.19	0.14
Yb_2O_3	0.10	0.07	0.08	0.09	0.08	0.07	n.d.	0.13	0.07	n.d.	0.08	0.10	0.11
Y_2O_3	1.82	0.70	0.94	1.83	0.59	2.51	3.41	2.94	2.12	2.19	2.36	2.59	2.98
Total	96.25	96.46	96.84	95.62	95.87	95.16	94.70	95.64	95.21	95.56	95.63	95.67	95.34
P	3.908	3.908	3.888	3.914	3.896	3.879	3.849	3.882	3.841	3.849	3.769	3.772	3.774
Si	0.033	0.029	0.033	0.024	0.024	0.052	0.079	0.052	0.068	0.048	0.143	0.117	0.123
total T	3.940	3.937	3.920	3.939	3.920	3.931	3.928	3.935	3.909	3.897	3.912	3.890	3.897
Ca	0.135	0.203	0.183	0.135	0.176	0.119	0.172	0.126	0.162	0.207	0.186	0.191	0.234
Th	0.116	0.147	0.157	0.090	0.140	0.104	0.176	0.112	0.182	0.196	0.275	0.233	0.250
U	0.022	0.034	0.034	0.039	0.033	0.024	0.043	0.027	0.018	0.030	0.012	0.011	0.014
Pb	0.004	0.005	0.005	0.005	0.005	0.004	0.005	0.003	0.005	0.005	0.006	0.005	0.005
La	0.783	0.797	0.788	0.801	0.808	0.807	0.755	0.785	0.794	0.771	0.753	0.756	0.731
Ce	1.666	1.686	1.666	1.704	1.710	1.710	1.580	1.667	1.690	1.638	1.635	1.647	1.571
Pr	0.188	0.185	0.199	0.187	0.198	0.197	0.182	0.187	0.185	0.195	0.191	0.196	0.185
Nd	0.763	0.752	0.769	0.743	0.763	0.697	0.664	0.705	0.694	0.696	0.660	0.701	0.704
Sm	0.138	0.128	0.132	0.122	0.128	0.121	0.119	0.121	0.126	0.130	0.115	0.115	0.118
Gd	0.130	0.123	0.106	0.123	0.118	0.116	0.118	0.117	0.113	0.118	0.110	0.105	0.115
Er			0.017		0.009	0.005	0.017	0.007	0.001	0.003	0.006	0.010	0.007
Yb	0.005	0.003	0.004	0.005	0.004	0.003		0.007	0.004		0.004	0.005	0.006
Y	0.159	0.061	0.083	0.161	0.052	0.222	0.303	0.258	0.189	0.194	0.211	0.231	0.266
XLREE	0.861	0.860	0.858	0.864	0.870	0.855	0.798	0.841	0.838	0.820	0.806	0.812	0.787
XHREE	0.033	0.031	0.031	0.031	0.032	0.030	0.033	0.032	0.028	0.029	0.029	0.029	0.030
Xhut	0.002	–0.004	0.003	0.000	0.000	0.003	0.013	0.004	0.010	0.006	0.026	0.014	0.008
Xbrb	0.066	0.098	0.088	0.066	0.085	0.058	0.083	0.061	0.078	0.099	0.089	0.091	0.111
$XYPO_4$	0.039	0.015	0.020	0.039	0.013	0.054	0.073	0.063	0.045	0.046	0.051	0.055	0.063
X(Y+HREE)	0.072	0.045	0.051	0.07	0.044	0.084	0.106	0.094	0.074	0.075	0.079	0.084	0.094

Sample NT-754-2: Coarse-grained granite-looking orthogneiss with aligned biotite and subhedral texture. The same locality as NT-753. The plagioclase is subhedral, entirely sericitized containing small secondary phengitic mica. K-feldspar (ca. 10 %) is mostly interstitial and finely perthitic. The biotite (10 %) dark red-brown to straw yellow, forms big flakes and encloses apatites, zircon and monazite. The flakes are weakly aligned. It contains small excluded ores, epidote–clinozoisite and secondary titanite. The muscovite (6 %) intergrows with biotite and is commonly cross-oriented. It has the composition of primary muscovite — relatively pure with high TiO_2 (max. 1.6 %). The Ti locally exsolves in lamellae of secondary rutile. Small phengitic mica replaces plagioclase cores. The accessories are represented by thick columnar apatite, ores by goethitized pyrrhotite. The monazite was found enclosed in biotite and quartz. This sample is characterized by the monazite breakdown to REE-clinozoisite (allanite), apatite and a Th phase (huttonite?) (Fig. 2A–B).

Sample NT-757: Massive, weakly banded biotite-garnet gneiss. Outcrop on the forest road in the Gelfúsová dolina Valley, elevation 975 m a.s.l. The plagioclase is sub- to anhedral, partly sericitized, bigger grains are slightly zoned. Basicity is An_{20-31}. Smaller grains are more basic. The biotite is very abundant (45 %) fresh, dark red-brown to straw yellow. It defines the banding of the rock. The garnet (2 %) is a characteristic metamorphic mineral, arranged in biotite bands, where it forms large (0.2–0.5 mm) anhedral, atol-like grains. In quartz-rich bands it is smaller and euhedral. The garnet is not altered. Sillimanite commonly intergrows with biotite, in places it is overgrown by muscovite. Myrmekite occurs occasionally. The accessories are abundant, plagioclase contains needle-like apatite, zircon and monazite. Biotite-hosted monazite (Fig. 3E–F) is surrounded by thin REE epidote rims. A xenotime was identified by microprobe.

Sample NT-761: Finely-banded orthogneiss of tonalite-granodiorite composition. The same locality as NT-27. The rock consists of quartz, plagioclase, biotite, muscovite and K-feldspar. The bands are 1–2 mm thick defined by micas. The dark red-brown biotite is abundant, fresh,

Table 2: *Continued.*

Sample	**NT-27**	**NT-27**	**NT-27**	**NT-27**	**NT-27**	**NT-761**	**NT-761**	**NT-761**	**NT-761**	**NT-761**	**NT-761**	**NT-761**	**NT-761**
Grain	m9-1	m9-2	m7-n2	m7-n3	m7-n4	m5-1	m5-2	m5-3	m5-4	m5-5	m8-3	m8-7	xen1-1
Age	324.8	367.0	448.4	505.1	491.7	323.2	306.8	320.7	410.2	334.0	324.7	328.1	n.d.
P_2O_5	26.43	26.95	28.07	29.19	28.23	28.34	28.57	28.64	28.32	27.86	29.68	29.18	32.56
SiO_2	0.85	0.56	0.38	0.48	0.40	0.64	0.23	0.26	0.60	0.57	0.21	0.44	1.33
CaO	1.02	0.79	1.79	2.27	2.24	1.44	1.35	1.38	0.83	0.95	1.24	0.58	0.03
ThO_2	7.01	4.95	9.29	10.85	10.95	6.45	5.57	5.70	5.32	5.43	5.58	3.67	0.97
UO_2	0.72	0.37	0.48	0.81	0.82	0.86	0.79	0.78	0.55	0.64	0.70	0.39	3.96
PbO	0.13	0.10	0.22	0.31	0.30	0.14	0.12	0.13	0.14	0.12	0.12	0.08	0.20
La_2O_3	12.02	12.80	10.80	9.40	9.83	12.61	12.23	12.09	13.11	12.83	12.41	13.93	n.d.
Ce_2O_3	25.47	27.25	25.26	24.03	24.26	25.95	26.44	26.47	26.63	26.34	26.94	27.76	0.04
Pr_2O_3	2.96	3.19	2.98	2.93	2.93	2.91	3.12	3.07	3.05	3.04	3.23	3.14	n.d.
Nd_2O_3	11.24	11.68	10.67	10.43	10.25	11.24	11.81	11.76	11.28	11.31	11.69	11.56	0.14
Sm_2O_3	2.06	1.90	2.39	2.53	2.63	2.14	2.22	2.40	2.20	2.22	2.19	2.00	0.28
Eu_2O_3	n.a.	n.a.	n.d.	n.d.	n.d.	n.d.	0.01	n.d.	n.d.	n.d.	n.d.	n.d.	0.57
Gd_2O_3	2.09	2.02	2.02	2.05	2.00	2.20	2.11	2.04	2.07	2.16	2.01	2.01	1.27
Tb_2O_3	n.a.	n.a.	0.17	0.15	0.16	0.17	0.13	0.14	0.17	0.15	0.15	0.15	0.37
Dy_2O_3	n.a.	n.a.	0.81	0.95	0.88	1.00	0.71	0.96	0.90	0.86	0.77	0.74	3.79
Ho_2O_3	n.a.	n.a.	0.28	0.15	0.29	0.13	0.08	0.15	0.18	0.17	0.21	0.06	1.23
Er_2O_3	0.18	0.17	0.02	0.22	0.11	0.19	0.26	0.08	0.17	0.14	0.06	0.11	4.29
Tm_2O_3	n.a.	n.a.	n.d.	0.04	n.d.	n.d.	n.d.	n.d.	n.d.	0.05	n.d.	0.01	0.68
Yb_2O_3	0.11	0.23	0.07	0.14	0.08	0.09	0.10	0.12	0.00	0.09	0.08	0.07	4.58
Lu_2O_3	n.a.	n.a.	0.05	n.d.	n.d.	n.d.	n.d.	n.d.	n.d.	n.d.	n.d.	0.05	0.62
Y_2O_3	2.67	2.22	2.92	2.84	2.64	3.16	2.71	2.90	2.76	3.22	2.53	2.63	41.05
Total	94.95	95.18	98.51	99.60	98.77	99.60	98.50	98.94	98.06	98.04	99.67	98.47	97.94
P	3.771	3.825	3.840	3.894	3.846	3.820	3.886	3.877	3.860	3.824	3.960	3.926	3.832
Si	0.143	0.093	0.062	0.076	0.065	0.101	0.036	0.041	0.097	0.092	0.036	0.070	0.184
total T	3.915	3.919	3.901	3.970	3.911	3.921	3.922	3.919	3.957	3.916	3.997	3.996	4.016
Ca	0.185	0.142	0.310	0.384	0.386	0.246	0.232	0.237	0.143	0.166	0.202	0.098	0.005
Th	0.269	0.189	0.341	0.389	0.401	0.234	0.204	0.208	0.195	0.200	0.193	0.133	0.031
U	0.027	0.014	0.018	0.029	0.030	0.031	0.029	0.029	0.020	0.024	0.022	0.014	0.122
Pb	0.006	0.004	0.009	0.012	0.012	0.006	0.005	0.005	0.006	0.005	0.005	0.004	0.008
La	0.747	0.792	0.644	0.546	0.583	0.741	0.725	0.713	0.779	0.767	0.720	0.816	
Ce	1.572	1.672	1.494	1.386	1.429	1.513	1.555	1.550	1.569	1.563	1.530	1.615	0.002
Pr	0.181	0.195	0.175	0.168	0.172	0.169	0.182	0.179	0.179	0.179	0.178	0.182	
Nd	0.677	0.699	0.616	0.587	0.589	0.639	0.677	0.671	0.648	0.655	0.656	0.656	0.007
Sm	0.120	0.110	0.133	0.137	0.146	0.117	0.123	0.132	0.122	0.124	0.121	0.109	0.013
Eu													0.027
Gd	0.117	0.113	0.108	0.107	0.106	0.116	0.113	0.108	0.111	0.116	0.111	0.106	0.059
Tb			0.009	0.008	0.008	0.009	0.007	0.007	0.009	0.008	0.007	0.008	0.017
Dy			0.042	0.048	0.045	0.052	0.037	0.049	0.046	0.045	0.039	0.038	0.17
Ho			0.015	0.007	0.015	0.007	0.004	0.007	0.009	0.009	0.013	0.003	0.054
Er	0.010	0.009	0.001	0.011	0.005	0.010	0.013	0.004	0.009	0.007	0.008	0.006	0.187
Tm				0.002						0.003		0.000	0.029
Yb	0.006	0.012	0.004	0.007	0.004	0.004	0.005	0.006		0.005	0.005	0.003	0.194
Lu			0.002									0.002	0.026
Y	0.239	0.198	0.251	0.238	0.226	0.268	0.231	0.247	0.237	0.277	0.204	0.222	3.037
XLREE	0.794	0.836	0.734	0.695	0.702	0.764	0.788	0.782	0.808	0.792	0.798	0.841	0.012
XHREE	0.032	0.032	0.043	0.047	0.044	0.047	0.043	0.044	0.045	0.046	0.046	0.041	0.185
Xhut	0.028	0.016	0.014	0.012	0.014	0.006	0.001	0.001	0.019	0.015	0.005	0.013	0.039
Xbrb	0.089	0.068	0.149	0.189	0.186	0.118	0.112	0.114	0.070	0.080	0.101	0.049	0.002
$XYPO_4$	0.058	0.048	0.06	0.058	0.054	0.064	0.056	0.059	0.058	0.067	0.051	0.055	0.762
X(Y+HREE)	0.089	0.080	0.104	0.105	0.099	0.112	0.099	0.103	0.103	0.113	0.096	0.097	0.946
T °C			636	640	621	659	622	635	634	662	614	615	-

commonly intergrown with muscovite the latter being also cross-oriented. As in sample NT-27 from the same locality, two varieties of K-feldspar (12 %) can be recognized: the larger perthitic K-feldspar concentrated in stripes is aligned along the foliation and may represent former augen. The non-perthitic K-feldspar with undulous extinction forms small anhedral pools suggesting the presence of partial melt. The sub- to anhedral sericitized plagioclase has basicity of An_{26}. The rock is rich in accessories, which are hosted mostly by biotite, and represented by monazite, zircon, xenotime and apatite (Fig. 3A–C). The monazite and zircon form distinct halos. The biotite-hosted monazite overgrows by thin REE-epidote rims.

Sample NT-764c: Biotite-muscovite-quartz-gneiss. Road cuts on the road Tále–Krpáčovo, elevation 840 m a.s.l., ca. 2.5 km NW from Bystrá dolina Valley. The rock is leucocratic composed mainly of quartz (50 %) and muscovite (15 %) with subordinate amount of biotite (9 %). The muscovite forms large flakes intergrown with biotite or cross-oriented. In places it forms fine symplectites with quartz. The biotite is dark-brown, pale yellow, fresh. Uncommon K-feldspar (3 %) occurs as subhedral perthitic crystals

(1.2 mm) and small interstitial non-perthitic crystals. The plagioclase is very rare (1 %), strongly retrogressed to sericite. Measurable places have basicity of An_{11}. The accessories are dominated by very common and large isometric apatite grains (up to 0.5 mm in size) commonly associated with muscovite. The monazite is small hosted by the apatite or micas (Fig. 2F).

Monazite

Occurrence of monazite

Orthogneisses contain monazite 40–120 μm in size, enclosed by biotite, plagioclase and quartz. The monazite in biotite seems to be least stable frequently showing a loss of LREE, and replacement of them by Y+HREE. In the sample NT-754-2 a more extensive replacement occurs, whereby monazite breaks down to form a secondary apatite enriched in Th and, along the biotite cleavage, REE-enriched epidote (allanite). The secondary apatite contains very small exsolutions of a Th mineral (huttonite?), which follow original boundaries of monazite (Fig. 2A,B). In orthogneisses NT-761, 754-2 xenotime was also found. Samples NT-12, 27 have monazites overgrown by REE-epidote rims, but monazite is still not replaced by apatite. The alteration only causes the formation of irregular dark domains enriched in Y and heavy REE. It is probably a variant of the monazite breakdown described by Broska & Siman (1998) and Finger et al. (1998). A difference is the formation of the Th silicate rimming apatite.

The monazite from paragneiss NT-757 forms isometric grains (30–50 μm) enclosed in biotite, plagioclase or

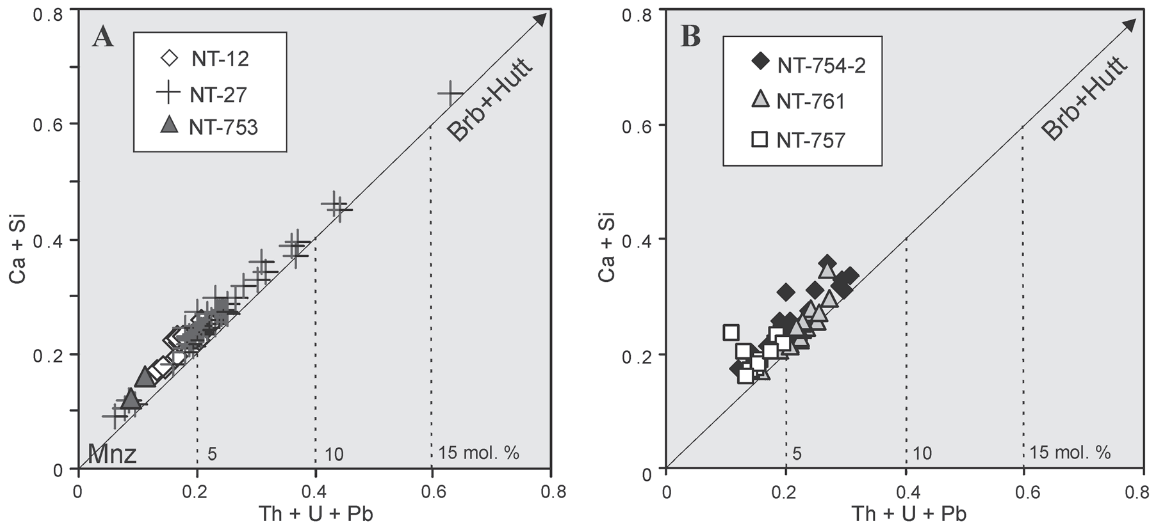

Fig. 4. The correlation Ca+Si vs. Th+U+Pb in studied monazites. Numbers refer to mol. % of brabantite (+huttonite).

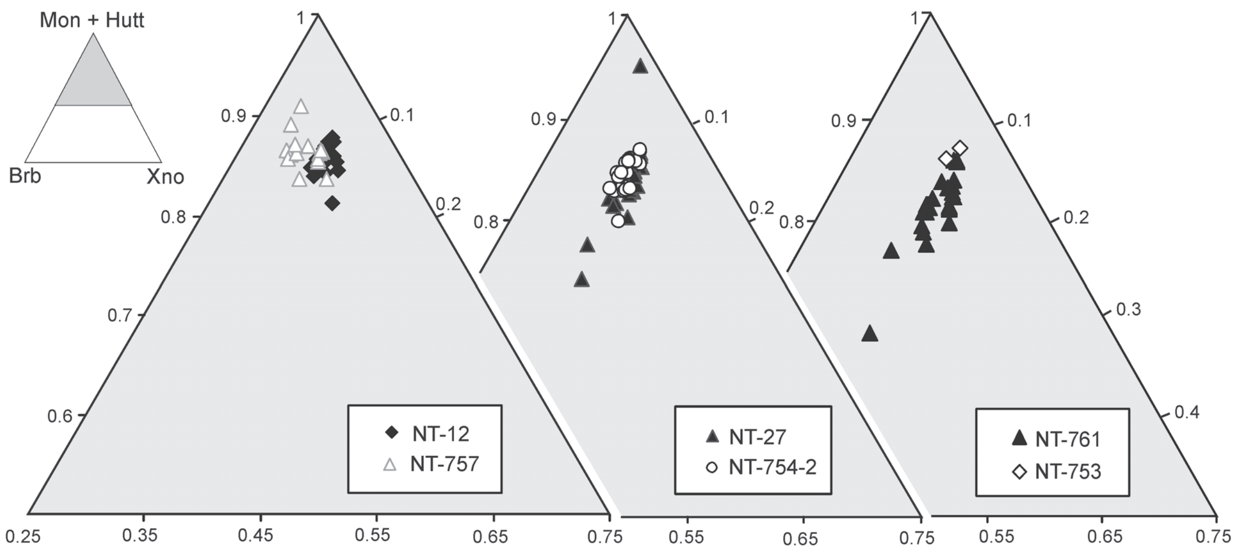

Fig. 5. Compositional range of studied monazites expressed in terms of end-members.

quartz. At rims it is frequently overgrown by allanite (or REE epidote), if located in biotite also by small secondary titanite. The secondary epidote rim in paragneisses is much thinner than in orthogneisses. Paragneiss NT-757 also contains xenotime and zircon.

Monazite chemical variability

The studied monazites are chemically characterized by ca. 140 analyses for 15–18 oxides (except NT-764c, Table 2). The chemical composition of monazite [$LREE(PO_4)$] is expressed in terms of solid solution end-members: huttonite $Th(SiO_4)$, brabantite $CaTh(PO_4)_2$ and xenotime $Y(PO_4)$. Monoclinic monazite is isostructural with huttonite and brabantite, and tetragonal xenotime is isostructural with zircon. Monazite compositional variation can be expressed by the following substitutions:

$2LREE^{3+} = (Th, U)^{4+} + Ca^{2+}$(Mnz→Brb), $LREE^{3+} + P^{5+} = (Th, U)^{4+} + Si^{4+}$(Mnz→Hutt) and $2LREE^{3+} = Y^{3+} + HREE^{3+}$(Mnz→Xno).

The first two substitutions correlate positively in coordinates (Th + U + Pb) *vs.* (Si + Ca) (Zhu & O'Nions 1999). From Fig. 4A,B it follows that these substitutions are responsible for the compositional variations of all monazites. The analyses are shifted above the correlation 1 : 1, probably due to slightly increased Ca. The largest compositional range (up to 16 mol. % of Hutt + Brb) has NT-27 augengneiss mainly due to high Th cores (see below). NT 754-2 and 761 are restricted to ca. 8 mol. % and monazites from NT-12, 757 to about 5 mol. %. The biotite schlier NT-753 hosts the purest monazite. Monazite composition in terms of (Mnz + Hutt)-Brb-Xno is shown in Fig. 5. Paragneiss monazite has 84–90 mol. % monazite, 6–10 mol. % of brabantite and 4–7 mol. % of xenotime. Orthogneiss mona-

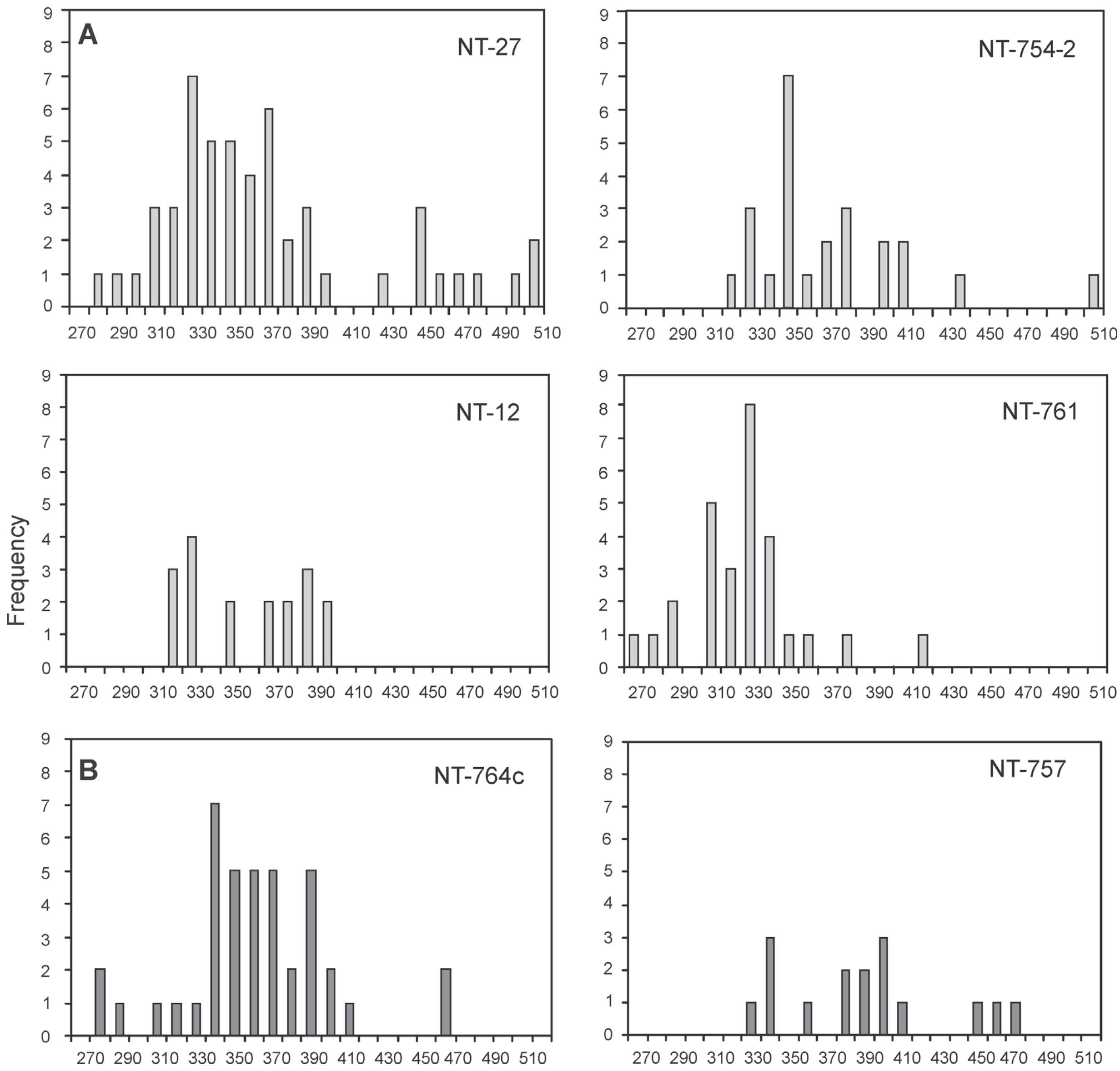

Fig. 6. Histograms of monazite ages: (A) orthogneisses (NT-27, 754-2, 12, 761), (B) paragneisses (NT-764c, 757).

Table 3: Results of electron microprobe dating of monazite. **m1-1** — monazite grain-spot, **an** — analysis. *Continued on the next pages.*

NT-	Grain	Th %	Y %	U %	Pb %	Pb 1σ	Th*	Ma	1σ
12	m1-1	2.417	1.665	0.497	0.0681	0.0086	4.051	380.6	47.8
12	m1-2	3.960	1.897	0.660	0.0851	0.0088	6.123	315.0	32.3
12	m2-1	4.297	1.644	0.479	0.0847	0.0087	5.873	325.3	32.8
12	m2-2	3.240	2.029	0.805	0.0990	0.0088	5.883	381.6	32.8
12	m3-1	4.303	1.615	0.449	0.0821	0.0088	5.782	320.6	34.2
12	m3-2	3.408	1.570	0.429	0.0682	0.0087	4.817	319.7	40.3
12	m3-3	3.932	1.781	0.630	0.0927	0.0087	6.002	348.8	31.9
12	m3-4	4.227	1.669	0.482	0.1072	0.0088	5.824	414.4	32.8
12	m4-1	3.355	1.658	0.486	0.0792	0.0088	4.954	360.9	39.4
12	m4-2	3.191	1.753	0.497	0.0776	0.0087	4.824	363.8	40.3
12	m4-3	3.088	2.087	0.804	0.0935	0.0087	5.724	370.3	33.8
12	m4-4	2.970	1.672	0.485	0.0762	0.0087	4.567	376.9	42.2
12	m5-1	3.236	1.793	0.601	0.0803	0.0087	5.207	348.8	37.0
12	m5-2	2.878	1.688	0.463	0.0640	0.0087	4.397	329.1	44.1
12	m6-1	2.411	1.977	0.601	0.0746	0.0086	4.385	385.3	43.1
12	m6-2	0.013	0.000	1.274	0.1216	0.0083	4.263	654.4	42.2
12	m6-3	4.068	2.683	1.039	0.1052	0.0089	7.464	320.2	26.7
12	m6-4	2.627	2.311	0.674	0.0660	0.0087	4.826	310.3	39.8
27	m1-1	5.071	1.886	0.464	0.1043	0.0089	6.606	355.3	29.5
27	m1-2	4.874	1.793	0.431	0.0949	0.0089	6.298	339.4	31.4
27	m2-1	5.256	2.118	0.673	0.1151	0.0090	7.472	347.8	26.7
27	m2-2	4.363	2.243	0.587	0.0853	0.0089	6.290	306.6	31.4
27	m3-1	4.339	1.827	0.504	0.1021	0.0087	6.006	383.4	31.9
27	m3-2	4.626	2.040	0.563	0.1064	0.0089	6.484	370.3	30.9
27	m4-1	4.887	1.743	0.539	0.1045	0.0088	6.666	353.4	29.1
27	m4-2	1.908	0.343	0.009	0.0414	0.0085	1.947	474.4	96.1
27	m4-3	6.880	1.581	0.251	0.1095	0.0091	7.726	318.3	25.8
27	m5-1	4.392	1.743	0.513	0.0915	0.0088	6.082	339.4	31.9
27	m5-2	4.606	1.763	0.356	0.0851	0.0088	5.784	330.9	33.8
27	m5-3	4.702	1.741	0.362	0.0957	0.0088	5.904	364.7	33.3
27	m6-1	5.974	2.288	0.828	0.1421	0.0089	8.701	368.4	22.5
27	m6-2	4.736	1.826	0.629	0.1049	0.0090	6.804	347.8	29.1
27	m7-1	4.110	1.677	0.514	0.0826	0.0088	5.800	321.6	33.8
27	m7-2	6.965	2.073	0.338	0.1623	0.0089	8.085	449.5	23.9
27	m7-3	3.984	1.748	0.474	0.1049	0.0087	5.553	425.6	34.7
27	m8-1	4.197	1.627	0.504	0.1003	0.0088	5.860	385.3	32.8
27	m8-2	4.135	1.929	0.457	0.0768	0.0087	5.637	307.5	34.2
27	m8-3	4.889	1.881	0.575	0.0985	0.0089	6.780	327.7	29.1
27	m9-1	6.157	2.102	0.657	0.1198	0.0091	8.321	324.8	24.4
27	m9-2	4.349	1.748	0.336	0.0892	0.0087	5.465	367.0	35.2
27	m9-3	5.178	1.833	0.463	0.1034	0.0088	6.708	346.9	29.1
27	m9-4	5.180	1.801	0.453	0.1046	0.0089	6.679	352.5	29.5
27	m9-5	3.697	1.719	0.389	0.0681	0.0087	4.976	308.4	38.9
27	m10	3.995	2.043	0.377	0.0749	0.0087	5.239	322.5	37.0
27	m11-1	5.806	2.063	0.588	0.1201	0.0090	7.746	349.7	26.3
27	m11-2	5.432	1.942	0.609	0.0906	0.0088	7.430	275.6	26.7
27	m12-1	4.427	1.893	0.345	0.0874	0.0088	5.571	353.0	35.2
27	m12-2	3.981	1.798	0.341	0.0891	0.0088	5.114	391.9	38.0
27	m13-1	3.819	1.800	0.404	0.0829	0.0088	5.154	362.8	38.0
27	m13-2	3.730	1.724	0.370	0.0732	0.0088	4.950	333.3	39.4
27	m13-3	4.786	1.969	0.509	0.1121	0.0089	6.471	390.0	30.5
27	m7 n1	4.034	2.041	0.482	0.0895	0.0051	5.605	360.1	22.6
27	m7 n2	8.160	2.301	0.431	0.1915	0.0054	9.573	448.4	14.5
27	m7 n3	9.539	2.233	0.737	0.2696	0.0056	11.97	505.1	12.3
27	m7 n4	9.621	2.080	0.747	0.2649	0.0056	12.08	491.7	12.1
27	m7 n5	8.317	2.322	0.443	0.2042	0.0055	9.772	467.9	14.4
27	m7 n6	8.215	2.375	0.441	0.1960	0.0054	9.664	454.5	14.5
27	m7 n7	3.921	1.907	0.502	0.0835	0.0050	5.555	339.3	22.6
27	m7 n8	4.627	2.227	0.529	0.1056	0.0051	6.354	374.5	20.2
27	m7 n9	5.428	2.269	0.621	0.1060	0.0051	7.445	321.4	17.2
27	m3 n1	4.123	1.990	0.481	0.0782	0.0050	5.686	310.7	21.9
27	m3 n2	3.412	1.940	0.389	0.0586	0.0050	4.674	283.0	26.2
27	m4 n1	2.166	0.169	0.018	0.0581	0.0049	2.226	580.5	56.7
27	m4 n2	1.852	0.218	0.014	0.0375	0.0048	1.897	441.0	64.1
27	m4 n3	1.449	0.212	0.001	0.0192	0.0048	1.451	295.4	187.4
27	m4 n4	13.93	2.115	0.550	0.2379	0.0056	15.69	340.1	9.1
27	m12 n1	4.479	1.869	0.368	0.0808	0.0050	5.676	320.9	21.9
27	m8 n1	3.924	1.876	0.422	0.0769	0.0050	5.295	327.8	23.4
27	m13 n1	4.768	2.008	0.496	0.1027	0.0051	6.384	362.5	19.9
27	m13 n2	4.884	2.169	0.587	0.0955	0.0051	6.790	317.6	18.6
753	m1	1.627	1.925	0.489	0.0497	0.007	3.188	354.4	50.6
753	m2	2.083	1.951	0.614	0.0590	0.007	4.040	331.9	39.8
754-2	m1-1	4.186	1.672	0.447	0.0955	0.0088	5.666	379.7	34.7
754-2	m1-2	4.542	1.722	0.730	0.1068	0.0089	6.939	347.8	28.1

zite is similar, showing a wider spread towards brabantite end-member (ca. 6–19 mol. %) and keeping 7–10 mol. % of xenotime. A lower xenotime is characteristic of paragneiss monazites which also show a low huttonite proportion (not shown).

Monazite Th correlates positively with U with average Th/U ratio 9.3 ± 4.1. Individual samples show similar values (NT-12 = 5.8 ± 1.7, NT-27 = 8.9 ± 1.7 and NT-761 = 7.7 ± 1). The exception is weakly foliated sample NT-754-2 with higher Th/U ratio 12.3 ± 6.3 due to lower U.

Dating results

All the age data are listed in Table 3. The ages obtained from the studied rocks are presented in histograms (Fig. 6A,B) for individual samples. The total number of analysed points is 196, all errors are 2 σ.

NT-12

The weighted average from 17 points measured on six monazites gives 349 ± 17 Ma (MSWD = 0.77). The monazites, mainly biotite-hosted, are commonly surrounded by epidote coronas. Th–U distribution is scattered monazites having lower Th compared to other samples. The Th-enriched corona epidotes (allanite) seem to act as Th sinks in this tonalitic rock. Th escape may be partly counterbalanced by of U influx, which is documented by the good correlation of U with Y. Y-enriched domains are darker and clearly indicate a later overprint.

NT-754-2

The age based on all 25 points from 11 grains gives a weighted average of 354 ± 15 Ma. The MSWD = 1.6 suggests a heterogeneous data set. Omitting seven outlying ages above 380 and below 310 Ma gives a new homogeneous set (n = 18) with a weighted average of 345 ± 13 Ma (MSWD = 0.48). The high ages (392–501 Ma) possibly indicate the presence of older monazite cores although they do not differ in composition from younger grains. Fig. 7A provides an isochron representation with the data divided into two groups. Both groups are well distinguished: while the younger set has almost zero intercept, the isochron age of the older set has a significant negative intercept and is clearly overestimated. The monazites hosted by biotite or muscovite are apparently not stable, they break down into the Th-enriched apatite and a corona of small grains of secondary huttonite(?). This breakdown may contribute to younging of the ages through opening of the system as suggested by the scattered Th–U distribution. Mona-

Table 3: *Continued.*

NT-	Grain	Th %	Y %	U %	Pb %	Pb 1σ	Th*	Ma	1σ
754-2	m1-3	6.343	1.860	0.287	0.1198	0.0089	7.306	368.0	27.2
754-2	m1-4	6.293	1.743	0.296	0.1206	0.0088	7.285	371.3	26.3
754-2	m2-1	5.376	2.042	0.258	0.1127	0.0089	6.243	405.0	31.9
754-2	m2-2	5.765	2.347	0.332	0.1045	0.0089	6.871	341.7	28.6
754-2	m3-1	2.923	1.924	0.283	0.0599	0.0086	3.857	349.7	49.2
754-2	m3-2	6.461	1.940	0.407	0.1141	0.0089	7.813	328.1	24.8
754-2	m4	3.917	2.061	0.778	0.1238	0.0089	6.484	431.3	30.0
754-2	m5	4.017	1.665	0.338	0.0909	0.0087	5.142	397.5	38.0
754-2	m6-1	3.619	1.812	0.189	0.0436	0.0086	4.244	231.6	45.0
754-2	m6-2	3.698	1.808	0.224	0.0777	0.0088	4.446	392.3	43.6
754-2	m6-3	4.284	1.626	0.322	0.0785	0.0088	5.352	330.0	36.6
754-2	m7-1	3.944	1.770	0.388	0.0813	0.0086	5.228	350.6	36.6
754-2	m7-2	3.667	1.552	0.394	0.0758	0.0088	4.965	344.1	39.4
754-2	m8	4.167	1.496	0.090	0.0685	0.0086	4.479	342.2	42.7
754-2	m9	4.993	1.388	0.393	0.0957	0.0089	6.296	342.2	31.4
754-2	m10	4.237	1.648	0.368	0.0978	0.0088	5.460	402.7	35.6
754-2	m11-1	4.298	1.552	0.515	0.0958	0.0088	5.998	360.5	32.8
754-2	m11-2	3.631	1.533	0.684	0.0983	0.0087	5.878	378.3	32.8
754-2	m11-3	2.503	1.633	0.248	0.0745	0.0087	3.332	501.6	57.2
754-2	m11 n1	3.928	2.345	0.460	0.0814	0.0051	5.424	338.6	23.2
754-2	m11 n2	3.978	1.747	0.619	0.0823	0.0051	5.987	310.9	21.0
754-2	m1 n1	6.616	1.896	0.311	0.1183	0.0051	7.628	348.2	16.8
754-2	m1 n2	4.294	1.744	0.430	0.0824	0.0051	5.693	326.4	22.0
757	m1	2.511	2.141	0.622	0.0816	0.0087	4.557	405.9	42.7
757	m2	2.090	1.336	0.448	0.0561	0.0085	3.557	357.2	53.4
757	m3-1	3.625	0.584	0.705	0.1044	0.0088	5.947	397.5	32.8
757	m3-2	2.734	1.481	0.691	0.0877	0.0087	5.005	397.0	38.4
757	m3-3	2.929	0.850	0.691	0.0766	0.0088	5.190	335.2	38.0
757	m4-1	2.948	0.348	0.377	0.0869	0.0087	4.199	465.9	45.9
757	m4-2	3.337	0.541	0.961	0.0969	0.0089	6.480	339.4	30.0
757	m5	2.791	1.378	0.674	0.0835	0.0088	5.004	378.3	38.9
757	m6-1	3.081	1.330	0.562	0.0819	0.0087	4.929	375.9	38.9
757	m6-2	3.790	0.506	0.615	0.0836	0.0087	5.805	325.8	33.3
757	m7-1	2.732	1.430	0.551	0.0917	0.0086	4.552	455.6	42.2
757	m7-2	2.983	1.418	0.591	0.0722	0.0087	4.919	332.3	39.8
757	m7-3	3.442	0.549	0.836	0.1079	0.0088	6.188	394.7	30.9
757	m8-1	3.679	0.742	0.831	0.1080	0.0088	6.407	381.6	30.5
757	m8-2	2.101	1.443	0.953	0.1017	0.0088	5.236	442.5	37.5
757	m8-3	3.239	0.465	0.798	0.0992	0.0087	5.858	383.4	32.8
761	m2-5	4.720	3.082	0.513	0.0783	0.0051	6.382	275.3	19.5
761	m3-6	3.580	1.995	0.343	0.0682	0.0050	4.695	325.4	26.2
761	m4 p1	5.318	2.585	0.732	0.1124	0.0051	7.696	327.5	16.5
761	m4 p2	5.587	2.691	0.834	0.1066	0.0052	8.290	288.6	15.3
761	m4 p3	6.855	2.525	0.912	0.1320	0.0052	9.813	301.9	13.1
761	m4 p4	4.434	2.387	0.600	0.1081	0.0051	6.391	378.7	19.9
761	m4 p5	6.157	2.477	0.809	0.1050	0.0051	8.776	268.8	14.2
761	m5 p1	5.672	2.490	0.776	0.1181	0.0052	8.195	323.2	15.7
761	m5 p2	4.897	2.130	0.715	0.0987	0.0051	7.218	306.8	17.3
761	m5 p3	5.011	2.281	0.707	0.1045	0.0051	7.308	320.7	17.3
761	m5 p4	4.674	2.176	0.500	0.1157	0.0052	6.310	410.2	20.5
761	m5 p5	4.768	2.531	0.578	0.0991	0.0050	6.649	334.0	18.8
761	m8/1	3.548	2.067	0.356	0.0738	0.0050	4.705	351.2	26.3
761	m8 p1	4.569	1.932	0.479	0.0850	0.0050	6.124	311.4	20.3
761	m8 p2	4.750	1.924	0.560	0.0963	0.0051	6.569	328.8	19.2
761	m8 p3	4.907	1.990	0.633	0.1008	0.0051	6.964	324.7	18.1
761	m8 p4	4.774	1.973	0.584	0.0835	0.0051	6.667	281.3	18.5
761	m8 p5	4.465	1.969	0.498	0.0823	0.0051	6.080	303.6	20.5
761	m8 p6	3.417	1.994	0.335	0.0622	0.0049	4.503	309.6	26.9
761	m8 p7	3.228	2.067	0.355	0.0642	0.0050	4.383	328.1	27.8
761	m8 p8	3.441	2.062	0.353	0.0688	0.0050	4.588	336.2	26.8
761	m8 p9	4.074	2.289	0.453	0.0839	0.0051	5.549	338.8	22.5
761	m8 p10	5.382	2.558	0.609	0.1063	0.0051	7.362	323.8	17.3
761	m8 p11	5.038	2.480	0.554	0.0993	0.0051	6.840	325.5	18.5
761	m8 p12	4.771	2.392	0.556	0.1008	0.0051	6.579	343.4	19.2
761	m8 p13	4.365	2.370	0.533	0.0839	0.0051	6.098	308.6	20.4
761	m8 p14	4.801	2.087	0.646	0.0969	0.0050	6.901	315.1	18.0
761	m8 p15	4.699	1.939	0.633	0.1017	0.0051	6.758	337.3	18.7
761	m8 p16	4.753	1.971	0.662	0.0983	0.0051	6.905	319.2	18.3
764c	m1-1	4.728	0.637	1.114	0.1128	0.0090	8.310	306.0	24.0
764c	m1-1	4.837	0.691	1.407	0.1379	0.0090	9.369	332.0	22.0
764c	m2-1	6.959	0.493	0.486	0.1377	0.0090	5.455	361.0	23.0
764c	m2-2	6.911	0.481	0.471	0.1358	0.0089	3.421	360.0	23.0
764c	m2-3	5.980	0.483	0.352	0.1217	0.0090	5.137	382.0	28.0
764c	m2-4	4.125	0.652	1.172	0.1199	0.0089	7.902	342.0	25.0

zites enclosed in quartz are more stable giving the age about 340 Ma.

NT-27

Thirteen grains from this sample were analysed by 52 points giving total weighted average 383 ± 19 Ma and high MSWD = 8.7. The data set splits into two groups in the histogram, the younger giving an average 340 ± 8 Ma, (n = 42, MSWD = 0.95). It shows two peaks at 320–330 Ma and 360–370 Ma. The older group (n = 10) gives 475 ± 19 Ma (MSWD = 2.3), six of these points come from one grain m-7 and show a high Th composition (7–9.5 % Th). The isochrons in Fig. 7B confirm both weighted averages having zero intercepts. Due to increased Ca the old core has brabantite content up to 15–19 mol. %. Monazites are hosted by all minerals, mostly by quartz and plagioclase, less by muscovite and biotite. The monazite ages do not differ in various hosts: 345 ± 13 Ma in biotite or muscovite, 341 ± 12 Ma in quartz and plagioclase (except the old core data). Quartz-hosted monazites seem to preserve a slightly older age (354 ± 13 Ma).

NT-761

Three grains were measured, one of them by a detailed profile. Twenty nine point ages give the weighted average 318 ± 11 Ma. The MSWD = 2.4 indicates a heterogeneous set. A detailed profile across m-8 monazite (17 points, Fig. 3B) also yields 322 ± 10 Ma and MSWD = 0.68. This euhedral grain is hosted by a K-feldspar pool, possibly indicating partial melt. All measured points define a non-disturbed correlation of Th vs. U (Th/U = 7.7 ± 1) which supports their younger age. The profile age is the same as the peak in the histogram, giving the weighted average 322 ± 8 Ma (MSWD = 0.46). The strongly foliated orthogneiss NT-761 thus may date the last deformation — a melting event with the lower age limit about 325 Ma.

NT-757, 764c

From the two metamorphic rocks sampled in remote localities (Gelfúsová dolina Valley and Tále–Krpáčovo, Fig. 1), we obtained 56 point data which split into three groups in histograms (Fig. 6B). The oldest group (n = 5) gives a weighed average of 454 ± 38 Ma (MSWD = 0.043). The old ages are found in both samples, always situated in the centers of monazite grains, and therefore, are considered inherited Ordovician cores. The main group of ages (n = 48) gives a well defined average of 355 ± 6 Ma (MSWD = 0.91). However, the base of the peak is 110 Ma (NT-764c), twice a value typical of monogenetic standard, which indicates

Table 3: *Continued from the page 237.*

NT-	Grain	Th %	Y %	U %	Pb %	Pb 1σ	Th*	Ma	1σ
764c	m2-5	4.097	0.658	1.594	0.1308	0.0091	9.229	321.0	22.0
764c	m3-1	5.417	0.347	1.297	0.1431	0.0092	7.157	336.0	21.0
764c	m4-1	2.662	1.014	0.500	0.0870	0.0087	4.287	456.0	45.0
764c	m4-2	3.505	1.034	0.702	0.0886	0.0089	5.770	346.0	35.0
764c	m4-3	2.026	1.163	0.424	0.0595	0.0087	3.398	394.0	57.0
764c	m4-4	1.965	0.980	0.432	0.0470	0.0086	10.16	316.0	57.0
764c	m4-5	3.323	0.591	0.551	0.0884	0.0087	5.105	389.0	38.0
764c	m4-6	3.518	0.633	0.588	0.0966	0.0088	5.421	400.0	36.0
764c	m5-1	4.800	0.709	1.637	0.1659	0.0092	10.09	371.0	20.0
764c	an1	4.084	1.754	0.595	0.1277	0.0075	6.041	476.0	27.4
764c	an2	3.183	1.144	0.295	0.0862	0.0073	4.153	466.2	38.7
764c	an3	0.139	0.125	0.028	0.0049	0.0050	0.231	483.9	474.0
764c	an4	5.322	0.534	1.103	0.1132	0.0074	8.864	288.6	18.5
764c	an5	7.773	0.382	0.691	0.1561	0.0076	10.02	350.7	16.9
764c	an6	4.080	0.494	1.439	0.0877	0.0073	8.680	229.5	18.8
764c	an7	2.893	1.369	0.731	0.0839	0.0072	5.276	360.7	30.5
764c	an8	3.978	0.957	0.548	0.0970	0.0073	5.766	379.6	28.2
764c	an9	2.325	1.274	0.631	0.0640	0.0072	4.378	331.9	36.4
764c	an10	2.062	1.278	0.441	0.0451	0.0071	3.478	293.1	45.7
764c	an11	3.410	0.650	0.569	0.0708	0.0073	5.238	304.8	31.1
764c	an12	4.362	0.648	0.533	0.0917	0.0073	6.095	339.5	26.4
764c	an13	4.354	0.443	0.600	0.0758	0.0071	6.277	272.5	25.2
764c	an14	5.622	0.536	0.712	0.1275	0.0075	7.942	362.1	20.9
764c	an15	5.888	0.578	0.555	0.1213	0.0074	7.696	355.1	21.4
764c	an16	5.471	0.691	1.444	0.1563	0.0075	10.17	348.8	16.5
764c	an17	2.211	0.550	1.524	0.1152	0.0070	7.179	366.9	21.6
764c	an18	6.075	0.539	0.556	0.1330	0.0074	7.890	379.5	20.8
764c	an19	5.576	0.645	1.254	0.1504	0.0076	9.660	353.0	17.4
764c	an20	5.540	0.638	1.220	0.1417	0.0075	9.511	337.9	17.4
764c	an21	3.086	0.550	1.111	0.1131	0.0072	6.714	383.1	23.7
764c	an22	4.865	0.333	0.602	0.1015	0.0072	6.823	335.7	23.6
764c	an23	0.376	0.114	0.599	0.0464	0.0059	2.343	454.0	55.5
764c	an24	2.896	0.567	1.644	0.0998	0.0073	8.173	277.6	20.0
764c	an25	6.551	0.467	0.512	0.1407	0.0075	8.223	384.6	20.2
764c	an26	6.758	0.442	0.348	0.0980	0.0071	7.874	279.6	20.1
764c	an27	5.293	0.721	0.966	0.1303	0.0075	8.438	349.6	19.7
764c	an28	5.480	0.580	0.461	0.1141	0.0074	6.982	367.7	23.5
764c	an29	10.79	0.619	0.928	0.2087	0.0078	13.81	340.3	12.6
764c	an30	6.198	0.441	0.575	0.1243	0.0074	8.070	347.1	20.3
764c	an31	4.522	0.479	0.532	0.0925	0.0073	6.251	334.0	26.1
764c	an32	3.694	0.502	0.552	0.0984	0.0073	5.497	404.1	29.3
764c	an33	4.010	0.708	1.928	0.1650	0.0076	10.30	365.4	16.5
764c	an34	3.998	0.659	1.269	0.1284	0.0075	8.134	358.8	20.6
764c	an35	16.52	0.385	0.810	0.2876	0.0083	19.15	337.3	9.6
764c	an36	12.77	0.462	0.687	0.2367	0.0080	15.01	354.1	11.8
764c	an37	11.80	0.514	0.864	0.2356	0.0079	14.62	362.5	12.1
764c	an38	4.897	0.671	1.526	0.1663	0.0076	9.878	382.4	17.0
764c	an39	6.136	0.587	0.427	0.0965	0.0074	7.506	289.0	21.8

that more than one age is recorded by the monazites. The distinct peaks around 330, 350 and 390 Ma are tentatively ascribed to the same three metamorphic events as recorded by metamorphic monazites from the Tatra Mts (Konečný et al. 2004). The youngest seems to correspond to the deformation — melting event of orthogneisses and migmatitization in the Vysoké Tatry Mts (Janák et al. 1999; Poller & Todt 2000).

Discussion

Y in monazite thermometry

Heinrich et al. (1997) and Pyle et al. (2001) found that the xenotime component in metamorphic monazite rises with temperature. Orthogneisses NT-761, NT-754-2 and paragneiss NT-757 contain xenotime, which buffers Y and makes it possible to use these empirical thermometers. The logarithmical fit of Pyle et al. (2001) is preferred because empirical data are calibrated against metamorphic temperatures and cover a wider range of $X_{(Y+HREE)}$. Compared to Heinrich et al. (1997) data, it yields temperatures lower by ca. 80 °C. The fit is given by the equation: T (°C) = 299.65*ln[$X_{(Y+HREE)}$] + 1315.2. Only analyses containing the same HREE (Gd, Dy Ho, Er and Yb) as in the original calibration were used. The NT-27 sample gives an average 613 ± 20 °C (n = 11, all errors due to range of Y + HREE). The profile in the m-8 grain shows a peak in Y contents and corresponding temperatures about 650 °C in centre of grain and ca. 600 °C at rims. The ages in the center vs. rim, however, do not differ significantly. The average for all 28 points is 625 ± 27 °C. Other orthogneiss samples with no xenotime found in thin sections, or incomplete HREE data give lower tem-

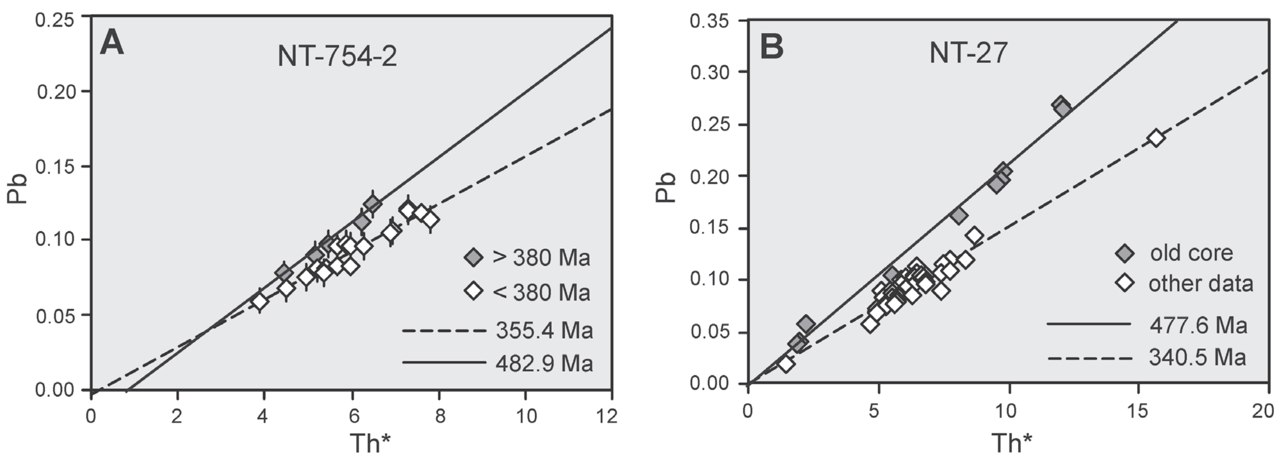

Fig. 7. Isochron diagrams of NT-27 and NT-754-2 orthogneisses. Bars indicate 1σ error of radiogenic lead concentrations (B), the same error is within the size of the symbols in (A). While zero intercepts in (A) confirm weighted averages, the negative intercept (–0.02) in (B) indicates an overestimation of the older group age.

peratures about 550 °C, which may be considered a low stability limit.

The paragneiss monazite has a significantly lower xenotime end-member: 4–8 mol. % (compared to 7–10 mol. % in orthogneisses). The difference is explained by the presence of garnet in biotite gneiss NT-757 where Y is partitioned between monazite and garnet. The increased Y in the rock is mineralogically documented by the occurrence of xenotime. The presence of latter means that garnet grows at buffered a_{YPO_4}. Pyle & Spear (2000) found that the Y concentrations in monazite coexisting with xenotime increase with temperature while those in garnet decrease. Y in garnet is at the detection limit of the microprobe in NT-757. The empirical equation of Pyle et al. (2001) gives temperatures between 380–530 °C with an average of 440 °C. They are considered to be the lower limit because Dy and Ho were not analysed in this monazite. The temperatures obtained in three orthogneiss samples do not correlate with the age (Fig. 8), which means that we cannot attribute an age to a metamorphic event.

Ages 440–500 Ma

The age about 460–490 Ma was initially indicated by two grains from sample NT-27. Repeated analyses situated close to the former points confirmed the old core of monazite m-7 (Fig. 2C,D). Moreover, the analyses showed that composition of the core differs significantly from the bulk of other monazites in higher Th/U ratio and increased brabantite proportion.

The Ordovician age is a characteristic age of orthogneisses from many Variscan domains. It is well documented from orthogneisses of the Moldanubian Zone of the Bohemian Massif (Gföhl gneiss; Friedl et al. 2004), southern Brittany (Brown & Dallmeyer 1996) or the Massif Central (Roger et al. 2004). Ordovician orthogneisses also occur in the Variscan basement involved in the Alpine orogen (Schultz et al. 2004). In the Western Carpathians Janák et al. (2002) obtained the age of 468 ± 24 Ma (chemical monazite method) from a northern Veporic metagranitoid which was metamorphosed under high P-T conditions at ca. 342 ± 27 Ma. Another Carpathian Ordovician rock is the Muráň gneiss from the southern Veporic Unit dated at 464 ± 35 Ma by zircon vapour digestion (UI, Gaab et al. 2005). A younger age of 405 ± 5 Ma was obtained for Západné Tatry (Western Tatra) orthogneiss (Poller et al. 2000). Putiš et al. (2001) dated zircons from trondhjemite associated with banded amphibolite (514 ± 24 Ma). The increasing recognition of pre-Variscan rocks suggests involvement of the Carpathian basement in the north Gondwana-derived Hun Superterran (von Raumer et al. 2002).

It is, therefore, tempting to ascribe the monazite age 475 ± 19 Ma to the age of Nízke Tatry orthogneisses as well. This, however, encounters problems: First, only one old core was actually found among 13 measured monazite grains, which otherwise give middle and late Variscan ages. Second, the composition of the old core is quite unique among the number of monazites analysed so far. Their high Th/U ratio 12–17 differs even more from the whole rock ratio (3–6), than the bulk of Variscan monazites which typically have ratios of 8.5–10. This suggests a different source rock and thus a restite rather than a magmatic origin of the old cores. A similar old age (ca. 500 Ma, Gurk 1999) was obtained from clastic metapelite zircons from the lower unit in the Západné Tatry Mts. Old cores (540–550 Ma) revealed by chemical monazite dating in Variscan (330 Ma) migmatites from the Cévennes area of the Massif Central (Be Mezeme et al. 2006) were recently interpreted as inherited.

The Ordovician age of granitic protolith of the orthogneiss would imply Early Paleozoic or Neo-Proterozoic wall rocks as are demonstrated in the Armorican massif or the Moldanubian Zone (Friedl et al. 2004). The old monazite cores found in biotite gneisses (440–480 Ma), therefore, seem to have been inherited and this age indicates rather, that the basin where the original protolith of para- and orthogneisses was sedimented, drained an area of a denudated Cadomian fundament.

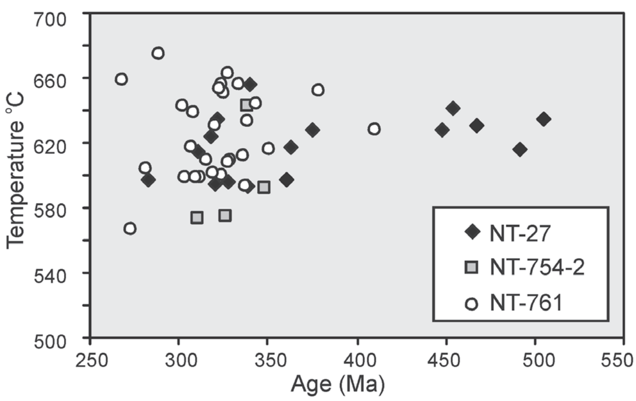

Fig. 8. Correlation of temperature after Pyle et al. (2001) with the age of monazite. Temperature was calculated only for points with analysed Gd, Dy, Ho, Er, Yb and Y.

Ages 340–350 Ma

The weighed averages of two samples (NT-12, 27, 754-2) falling within the interval 340–350 Ma are based on the largest number of measurements (60). This would mean that the dominant mass of monazite formed and/or recrystallized at this time implying the Variscan age of the parental rock. The points forming a small peak at 380–390 Ma were checked in view of the existing discordant zircon age 381 ± 6 Ma (Putiš et al. 2003). However, repeated measurements located closest to original points failed to confirm this age, producing younger data. The period 340–360 Ma is the age of the main Variscan collision in the Western Carpathian basement when, earlier in this interval, a medium-P metamorphism took place followed by syncollisional S-type granites intrusions at ca. 350 Ma (Poller et al. 2000; Poller & Todt 2000; Finger et al. 2003).

On the other hand, syntectonic orthogneisses should pre-date the post-tectonic undeformed Nízke Tatry tonalite (Ďumbier type) dated at 343±3 Ma by Putiš et al. l.c., and 330±10 Ma by Poller et al. (2001) by common lead. Resolution of monazite chemical dating with the typical base of age peak corresponding to 60 Ma does not allow us to establish a precise intrusion age. Since monazites recrystallized at a lower temperature (ca. 600–650 °C) compared to zircon, the obtained interval of 340–350 Ma is considered a lower limit for orthogneiss formation.

Ages 320–330 Ma

Distinguishing between the monazite ages of about 350 and 330 is clearly at the edge of the chemical method possibilities, the distinct peaks in both ortho- and paragneisses (Fig. 6) nevertheless suggest a thermal event ca. 330 Ma ago. The foliated orthogneiss NT-761 gives such a younger age (325±10 Ma) which may record the same event as is documented by numerous zircon and monazite data from the Western Carpathians (Poller & Todt 2000; Poller et al. 2001; Finger et al. 2003). During this post-collisional event many I-type granitoids were emplaced in Tatric and Veporic Units. The thermal event which produced these granitoids was accompanied by rapid uplift and decompression melting. Such melting was documented in the Západné and Vysoké Tatry (High Tatra) migmatite (orthogneiss?) by Janák et al. (1999) and dated at 332±5 Ma by Poller & Todt (2000). An analogical situation is suggested by monazite data from the Nízke Tatry orthogneisses. The sample NT-761 seems to have been remelted *via* muscovite dehydration melting. It contains new K-feldspar, apparently a product of the reaction: $Mu + Qtz = Kfs_{melt} + Sill$ (650–700 °C and 600–700 MPa, Spear et al. 1999). The Y in monazite indicates an average temperature of 601±75 °C (Pyle et al. 2005, error due to range of Y), which means that it largely recrystallized later, in subsolidus conditions. The 330 Ma event, which is also recorded by metamorphic monazites, appears important in the Nízke Tatry Mts. The same age, 330 Ma, obtained also by muscovite $^{40}Ar/^{39}Ar$ dating (Dallmeyer et al. 1993) suggests a phase of rapid cooling following the decompression (Brown & Dallmeyer 1996).

Conclusions

Monazite compositions from both the orthogneiss and paragneiss of the Nízke Tatry Mts reflect their respective meta(sedimentary) protoliths. The main substitutions in both rock types are monazite–xenotime (max. 11.5 mol. %) and monazite–brabantite (max. 11.8 mol. %, the old core in NT-27 up to 19 mol. %), and to a lesser extent monazite–huttonite (max. 3 mol. %). Monazites from all orthogneisses appear unstable, showing local escape of the light REE, which are captured in REE-epidote rims. In more advanced degrees of the alteration monazite breaks down to Th-enriched apatite, REE-epidote and huttonite(?).

Extensive chemical dating of the monazite from Nízke Tatry orthogneisses has shown that monazite can record both old events in its cores and younger history in overgrown and/or recrystallized rims. The overwhelming mass of monazite gives Variscan ages between 340–350 Ma indicating a strong Variscan reworking including partial melting. The reason why monazite failed to record reliably a primary age of the syn-tectonic intrusion probably results from its recrystallization, which seems to have occurred at relatively low temperatures, typically between 600–660 °C. Although dissolution–precipitation processes culminated 350–340 Ma ago, the points giving range between 380–440 may remember older processes. The well defined old cores (ca. 480 Ma) found in one orthogneiss sample are at present too scarce to give a solid basis for a primary Ordovician age of the orthogneisses, even though this possibility cannot be entirely dismissed.

Monazite from one strongly foliated sample also records a younger event at ca. 330 Ma which is interpreted as the end of the decompression phase (at 600 °C) and beginning of the phase of rapid isobaric cooling. This is corroborated by the coincidence of monazite and muscovite $^{40}Ar/^{39}Ar$ ages. The muscovite is thought to have formed during retrogression of the orthogneisses after the phase of partial decompression melting. Such a P-T path is characteristic of many Variscan plutons in the Western Carpathians (Malá Fatra, Kohút et al. 1997; Tatra Mts, Janák et al. 1999) and other Variscan domains (southern Armorica, Brown & Dallmeyer 1996).

Acknowledgment: This work was supported by the Project GA-4096 (VEGA, Slovak Grant Agency) and Project 45s6 (Aktion Österreich–Slowakei) to I.P. All reviewers F. Finger, I. Broska and M. Janák are acknowledged for critical reading of an earlier version of the manuscript. F. Finger is thanked for his invaluable help with microprobe dating work.

References

Adamija S., Abesadze M., Chkhouta T., Kekelia M. & Tsimakuridze G. 1992: Tectonites in the Variscan crystalline assemblages of the Greater Caucasus and Ďumbier Massif of Western Carpathians. In: Vozár J. (Ed.): Palaeozoic geodynamic domains in the Tethys. *GÚDŠ*, Bratislava, 7–19.

Be Mezeme A., Cocherie A., Faure M., Legendre O. & Rossi Ph. 2005: Electron microprobe monazite geochronology of magmatic events: examples from Variscan migmatites and granitoids, Massif Central, France. *Lithos* (article in print).

Bezák V. & Biely A. 1998: Geological-tectonical structure of the Ďumbier part of the Nízke Tatry and parallels with the Andrusov et al. (1951) study. *Miner. Slovaca* 30, 81–83 (in Slovak).

Bezák V. & Klinec A. 1998: The new interpretation of tectonic development of the Nízke Tatry Mts. — West part. *Geol. Zbor. Geol. Carpath.* 31, 569–575.

Broska I. & Siman P. 1998: The breakdown of monazite in the West Carpathian Veporic orthogneisses and Tatric granites. *Geol. Carpathica* 49, 161–167.

Braun I., Montel & J.-M. Nicollet Ch. 1998: Electron microprobe dating of monazites from high-grade gneisses and pegmatites of the Kerala Khondalite belt, southern India. *Chem. Geol.* 146, 65–85.

Brown M. & Dallmeyer R.D. 1996: Rapid Variscan exhumation and the role of magma in core complex formation: southern Brittany metamorphic belt, France. *J. Metamorphic Geology* 14, 361–379.

Cherniak D.J., Watson E.B., Grove M. & Harrison T.M. 2004: Pb diffusion in monazite: A combined RBS/SIMS study. *Geochim. Cosmochim. Acta* 68, 829–840.

Crowley J.L. & Ghent E.D. 1999: An electron microprobe study of the U-Th-Pb systematica of metamorphosed monazite: the role of Pb diffusion versus overgrowth and recrystallization. *Chem. Geol.* 157, 285–302.

Dallmayer R.D., Neubauer F., Fritz H. & Putiš M. 1993: Variscan vs. Alpine tectonothermal evolution within the Eastern Alps and Western Carpathians, Austria–Slovakia. *Geol. Carpathica* 44, 255–256.

Finger F., Broska I., Roberts M. & Schermaier A. 1998: Replacement of primary monazite by apatite-allanite-epidote coronas in an amphibolite facies granite gneiss from the Eastern Alps. *Amer. Mineralogist* 83, 248–258.

Finger F. & Broska I. 1999: The Gemeric S-type granites in southeastern Slovakia: Late Palaeozoic or Alpine intrusions? Evidence from electron microprobe dating of monazite. *Schweiz. Mineral. Petrogr. Mitt.* 79, 439–443.

Finger F. & Faryad S.W. 1999: A Variscan monazite age from the Zemplín basement (eastern Western Carpathians). *Acta Geol. Hung.* 42, 301–307.

Finger F., Broska I., Haunschmid B., Hraško Ľ., Kohút M., Krenn E., Petrík I., Riegler G. & Uher P. 2003: Electron-microprobe dating of monazites form Western Carpathian basement granitoids: plutonic evidence for an important Permian rifting event subsequent to Variscan anatexis. *Int. J. Earth Sci.* 92, 86–98.

Foster G., Gibson H.D., Parrish R., Horstwood M., Fraser J. & Tindle A. 2002: Textural, chemical and isotopical insights into the nature and behaviour of metamorphic monazite. *Chem. Geol.* 191, 183–207.

Friedl G., Finger F., Paquette J.-L., von Quadt A., McNaugthon N.J. & Fletcher I.R. 2004: Pre-Variscan geological events in the Austrian part of the Bohemian massif deduced from U-Pb zircon ages. *Int. J. Earth Sci.* 93, 802–823.

Fritz H., Neubauer F., Janák M. & Putiš M. 1992: Variscan mid-crustal thrusting in the Carpathians. Part II: Kinematics and fabric evolution of the Western Tatra basement. *Terra Abstr. Suppl.* 2, 4, 24.

Gaab A.S., Janák M., Poller U. & Todt W. 2005: Alpine reworking of Ordovician protoliths in the Western Carpathians: Geochronological and geochemical data on the Muráň gneiss complex, Slovakia. *Lithos* (article in print).

Gurk Ch. 1999: Petrographie, Geochemie and Geochronologie der unteren Einheit, Tatricum, Westliche Tatra (Slowakei). *Manuscript,* Universität Mainz, 1–124.

Harlov D.E., Wirth E. & Förster H.-J. 2005: An experimental study of dissolution–reprecipitation in fluorapatite: fluid infiltration and the formation of monazite. *Contr. Mineral. Petrol.* 150, 268–286.

Heinrich W., Andrehs G. & Franz G. 1997: Monazite–xenotime miscibility gap thermometry. I. Empirical calibration. *J. Metamorph. Geology* 15, 3–16.

Janák M. 1994: Variscan uplift of the crystalline basement, Tatra Mts., Central Western Carpathians: Evidence from $40^{Ar}/39^{Ar}$ laser probe dating of biotite and P-T-t paths. *Geol. Carpathica* 45, 293–300.

Janák M., Chovan M., Smirnov A. & Majzlan J. 2000a: Kyanite and sillimanite in gneisses of Ďumbier crystalline complex, the Low Tatra Mountains. In: Uher P., Broska I., Jeleň S. & Janák M. (Eds.): Magurka 2000. *Geol. Inst. SAS,* Bratislava, 15.

Janák M., Pitoňák P. & Spišiak J. 2000b: Garnet-clinopyroxene metabasites from Jasenie, Low Tatra Mountains. In: Uher P., Broska I., Jeleň S. & Janák M. (Eds.): Magurka 2000. *Geol. Inst. SAS,* Bratislava, 14.

Janák M., O'Brien P.J., Hurai V. & Reutel C. 1996: Metamorphic evolution and fluid composition of garnet-clinopyroxene amphibolites from the Tatra Mountains, Western Carpathians. *Lithos* 39, 57–79.

Janák M., Hurai V., Ludhová L., O'Brien P.J. & Horn E.E. 1999: Dehydration melting and devolatilization during exhumation of high-grade metapelites: the Tatra Mountains, Western Carpathians. *J. Metamorph. Geology* 17, 379–395.

Janák M., Finger F., Plašienka D., Petrík I., Humer B., Méres Š. & Lupták B. 2002: Variscan high P-T recrystallization of Ordovician granitoids in the Veporic unit (Nízke Tatry Mountains, Western Carpathians): new petrological and geochronological data. *Geolines* 14, 38–39.

Konečný P., Siman P., Holický I., Janák M. & Kollárová V. 2004: Methodics of monazite dating using an electron microprobe. *Miner. Slovaca* 36, 225–235 (in Slovak).

Kohút M. 2004: Orthogneisses of the Western Carpathians — a survey of present knowledge. *Miner. Slovaca* 36, 141–155.

Kohút M., Todt W., Janák M. & Poller U. 1997: Thermochronometry of the Variscan basement exhumation in the Veľká Fatra Mountains (Western Carpathians, Slovakia). *Terra Nova, Abstr. Suppl.* 9, 1, 494.

Ludwig K.R. 2001: User manual for Isoplot/Ex ver. 2.49. A geochronological toolkit for Microsoft Excel. *Berkeley Geochronological Centre Spec. Publ.* 1a, 1–56.

Méres Š. & Hovorka D. 1992: Albite — microcline orthogneisses of the Tríbeč Mts. *Miner. Slovaca* 24, 349–356.

Madarás J., Putiš M. & Hók J. 1999: Structural features of the Hercynian tectonics in the southern part of the Ďumbier crystalline complex (Nízke Tatry Mts., Western Carpathians). *Miner. Slovaca* 31, 17–30.

Miko O. & Lukáčik E. 1983: Petrography of crystalline complex rocks, northwest of Kyslá, at Jasenie. In: Pecho J. & Molák Pulec M. (Eds.): Scheelite-gold ore mineralization in the Nízke Tatry. *GÚDŠ*, Bratislava, 39–47.

Montel J-M., Foret S., Veschambre M., Nicollet Ch. & Provost A. 1996: Electron microprobe dating of monazite. *Chem. Geol.* 131, 37–53.

Parrish R.R. 1990: U-Pb dating of monazite and its application to geological problems. *Canad. J. Earth Sci.* 27, 1431–1450.

Petrík I., Siman P. & Bezák V. 1998: Granitoid protolith of orthogneisses from the Ďumbier Nízke Tatry Mts. — Distribution of barium in megacrysts of K-feldspar. *Miner. Slovaca* 30, 265–274 (in Slovak).

Poitrasson F., Chenery S. & Bland D.J. 1996: Contrasted monazite hydrothermal alteration mechanisms and their geochemical implications. *Earth Planet Sci. Lett.* 145, 79–96.

Poitrasson F., Chenery S. & Shepherd T.J. 2000: Electron microprobe and LA-ICP-MS study of monazite hydrothermal alteration: Implications for U-Th-Pb geochronology and nuclear ceramics. *Geochim. Cosmochim. Acta* 64, 3283–3297.

Poller U., Janák M., Kohút M. & Todt W. 2000: Early Variscan magmatism in the Western Carpathians: U-Pb zircon data from granitoids and orthogneisses of the Tatra Mountains (Slovakia). *Int. J. Earth Sci.* 89, 336–349.

Poller U. & Todt W. 2000: U-Pb single zircon data of granitoids from the High Tatra Mountains (Slovakia): implications for the geodynamic evolution. *Trans. Roy. Soc. Edinburgh, Earth Sci.* 91, 235–243.

Poller U., Todt W., Kohút M. & Janák M. 2001: Nd, Sr, Pb isotope study of the Western Carpathians: implications for Palaeozoic evolution. *Schweiz. Mineral. Petrol. Mitt.* 81, 159–174.

Putiš M., Kotov A.B., Petrík I., Korikovsky S.P., Salnikova E.B., Yakovleva S.Z., Berezhnaya N.G., Kovach V.P. & Plotkina

Y.V. 2001: U-Pb zircon ages of dioritic and trondhjemitic rocks from a layered amphibolitic complex crosscut by granite vein (Veporic basement, Western Carpathians). *Geol. Carpathica* 52, 49–60.

Putiš M., Kotov A.B., Petrík I., Korikovsky S.P., Madarás J., Salnikova E.B., Yakovleva S.Z., Berezhnaya N.G., Plotkina Y.V., Kovach V.P., Lupták B. & Majdan M. 2003: Early vs. late-orogenic granitoids: structural, age and petrological relationships in the Variscan basement (Nízke Tatry and Malá Fatra Mountains, Slovakia). *Geol. Carpathica* 54, 163–174.

Pyle J.M. & Spear F.S. 2000: An empirical garnet (YAG)-xenotime thermometer. *Contr. Mineral. Petrol.* 138, 51–58.

Pyle J.M., Spear F.S., Rudnick R.L. & McDonough W. 2001: Monazite-xenotime-garnet equilibrium in metapelites and a new monazite-garnet thermometer. *J. Petrology* 42, 2083–2107.

von Raumer J.F., Stampfli G.M., Borel G. & Bussy F. 2002: Organization of pre-Variscan basement areas at the north-Gondwanan margin. *Int. J. Earth Sci.* 91, 35–52.

Roger F., Respaut J.-P., Brunel M., Matte Ph. & Paquette J.-L. 2004: Première datation U-Pb des orthogneiss oeillés de la zone axiale de la Montagne Noire (Sud du Massif central): nouveaux témoins du magmatisme ordovicien dans la chaîne Varisque. *C. R. Geoscience* 336, 19–28.

Schultz B., Bombach K., Pawlig S. & Brätz H. 2004: Neoproterozoic to Early-Palaeozoic magmatic evolution in the Gondwana-derived Austroalpine basement to the south of the Tauern window (Eastern Alps). *Int. J. Earth Sci.* 93, 824–843.

Simpson R.L., Parrish R.P., Searle M.P. & Waters D.J. 2000: Two episodes of monazite crystallization during metamorphism and crustal melting in the Everest region of the Nepalese Himalaya. *Geology* 28, 403–406.

Spišiak J. & Pitoňák P. 1990: The Nízke Tatry Mts. crystalline complex — new facts and interpretation (West Carpathians, Czechoslovakia). *Geol. Zbor. Geol. Carpath.* 41, 377–392.

Spear F.S., Kohn M.J. & Cheney J.T. 1999: P-T paths from anatectic pelites. *Contr. Mineral. Petrol.* 134, 17–32.

Townsend K.J., Miller C.F., D'Andrea J.L., Ayers J.C., Harrison T.M. & Coath C.D. 2000: Low temperature replacement of monazite in the Ireteba granite, Southern Nevada: geochronological implications. *Chem. Geol.* 172, 95–112.

Vavra G. & Schaltegger U. 1999: Post-granulite facies monazite growth and rejuvenation during Permian to Lower Jurassic thermal and fluid events in the Ivrea Zone (Southern Alps). *Contr. Mineral. Petrol.* 134, 405–414.

Zhu X.K. & O'Nions R.K. 1999: Zonation of monazite in metamorphic rocks and its implications for high temperature thermochronology: a case study from the Lewisian terrain. *Earth Planet. Sci. Lett.* 171, 209–220.